EO Science Strategy Foundation Study:

D5: Links between Candidate Science Questions, Geophysical Observables and EO mission capabilities

This deliverable describes the linkage between the Geophysical Observables required by the Candidate Science Questions (CSQs) and the capabilities of existing and planned EO Missions. It also describes the approach to, and results of, a high-level capability gap analysis, and examples of a detailed capability gap analysis for three of the CSQs. It should be read in conjunction with deliverable D2, which describes the CSQs themselves.

April 2024

Cover + 45 pages

Symbios Communications

Table of Contents

Revision History

Version	Notes
v1.0	Release date: 24 November 2023 Authors: G. Dyke, L. Rose, J. Muir, S. Ward
v1.1	Release date: January 2024 *Updates to reflect feedback and discussion at PM2.*
v1.2	Release date: April 2024 *Reflected updated CSQ to observables mapping, feedback and discussion around Final Presentation. Addition of detailed gap analyses for three CSQs* Authors: G. Dyke, L. Rose, J. Muir, S. Ward (Symbios) D. Crisp (Crisp Spectra) M. Herold (GFZ) A. Hogg (University of Leeds) J. Johannessen (NERSC) G. Lopez-Saldana (Assimila)

Table of Acronyms

Acronym	Expansion
CSQ	Candidate Science Question
EO	Earth observation
GO	Geophysical Observable
KAO	Knowledge Advancement Objective
SSFS	Science Strategy Foundation Study

1: Objectives and Outputs

This document is deliverable D5 from the ESA EO Science Strategy Foundation Study (SSFS). It describes the linkage between the Geophysical observables required by the Candidate Science Questions (CSQs) and the capabilities of existing and planned EO Missions. It also describes the approach to and results of a high-level capability gap analysis, and examples of a detailed gap analysis for three of the CSQs.

The outputs of Deliverable 5 include:

- a table of all the Geophysical Observables (GO) required by the CSQs
- an initial analysis of the GOs to help characterise the information gathered
- a set of sheets for the high priority GOs showing an initial capability gap analysis compared to the capacity of existing and planned EO missions (contained in Appendix C which is a separate document)
- Examples of a more detailed gap analysis undertaken for 3 of the CSQs.

Full details of the CSQs are contained in Deliverable D2.

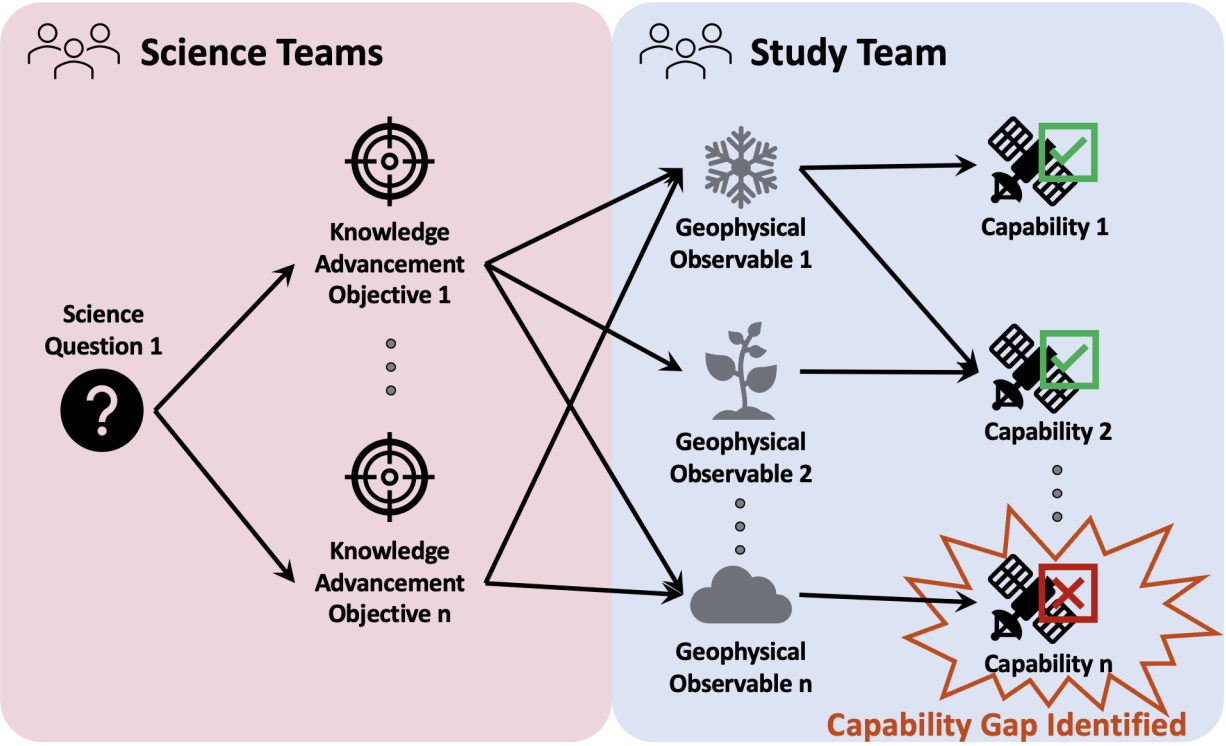

Figure 1: Overall SSFS Task 2 Process Summary where each Science Question is decomposed into Knowledge Advancement Objectives that are then mapped to Geophysical Observables, and then to capabilities via CEOS Database measurements or OSCAR/Variables

2: Methodology

As a part of the overall approach to the SSFS, a number of Candidate Science Questions (CSQs) were developed, covering a wide range of topics. The CSQs were intentionally cross-disciplinary, with differing

scale and breadth, covering major questions in Earth system science. An initial set of 57 CSQs was developed, and Deliverable 6 describes the process and criteria for narrowing them down to 22 for detailed assessment of required geophysical observables under this Deliverable 5 (see Figure 2). A list of the CSQs addressed by this deliverable is provided in Section 3.

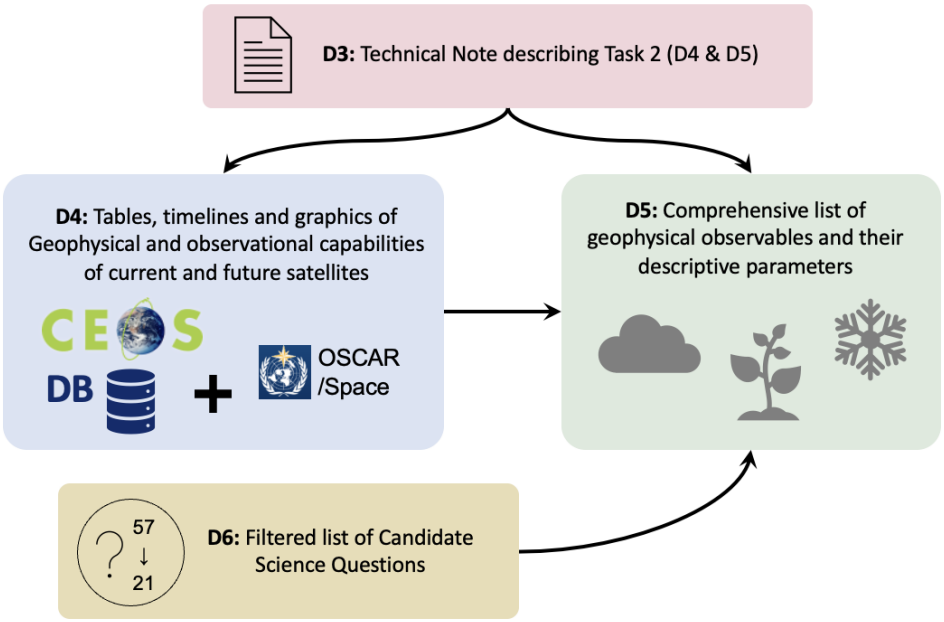

Figure 2: Linkage between Deliverables 3, 4, 5 and 6

For each of the CSQs, detailed science sheets were developed in consultation with the study science teams. Initially versions included all 57 of the CSQs, with a second iteration being performed by the study team and science teams for the 22 CSQs selected for detailed assessment. An example of a science sheet is provided in Appendix A, with the full set is provided in SSFS Deliverable D2.

As a part of this second iteration, the CSQs and their Knowledge Advancement Objectives (KAOs) were mapped to capabilities captured in the sources noted in Table 1 below.

Source	**Number of Geophysical Observables Mapped**
CEOS Database *database.eohandbook.com/measurements/overview.aspx*	128
OSCAR Variables *https://space.oscar.wmo.int/variables*	10
Unmapped *See Appendix B*	54

Table 1: Count of distinct Geophysical Observable mapped to CEOS Database measurements, OSCAR/Variables, or unmapped to either

The science teams were also asked to identify a priority level for the GO they identified, shown in Table 2.

Priority Level	**Number**
Critical *A Geophysical Observable that is uniquely enabling to address the CSQ above and beyond current capabilities.*	411
Supporting *Other Geophysical Observables which are ancillary to those above which are assumed to be routinely available.*	459
Total	**870**

Table 2: Count of Geophysical Observable mapped by priority level

Based on the inputs from the science teams, and iteration with the study team, a table mapping the CSQ, KAO, GO identified, and where available measurement specifications were generated. This is delivered as a separate Excel document, with an example shown in Table 3 below.

CSQ ID	KAO ID	Geophysical Observable	Priority Level	Specification Text Summary
1	A	CO2 Mole Fraction	Critical	High-spectral-resolution imaging spectroscopy of CO2, CH4 and O2 bands at 1-10 km spatial resolution with 0.1 to 0.5% accuracy. High-spatial-resolution multi-spectra/hyperspectral CO2, CH4 observations with accuracies of 1-2% on spatial scales 0.01 to 1 km.
1	A	CO2 Total Column	Critical	High-spectral-resolution imaging spectroscopy of CO2, CH4 and O2 bands at 1-10 km spatial resolution with 0.1 to 0.5% accuracy. High-spatial-resolution multi-spectra/hyperspectral CO2, CH4 observations with accuracies of 1-2% on spatial scales 0.01 to 1 km.
1	A	CH4 Mole Fraction	Critical	High-spectral-resolution imaging spectroscopy of CO2, CH4 and O2 bands at 1-10 km spatial resolution with 0.1 to 0.5% accuracy. High-spatial-resolution multi-spectra/hyperspectral CO2, CH4 observations with accuracies of 1-2% on spatial scales 0.01 to 1 km.
1	A	CH4 Total Column	Critical	High-spectral-resolution imaging spectroscopy of CO2, CH4 and O2 bands at 1-10 km spatial resolution with 0.1 to 0.5% accuracy. High-spatial-resolution multi-spectra/hyperspectral CO2, CH4 observations with accuracies of 1-2% on spatial scales 0.01 to 1 km.
1	B	CO2 Mole Fraction	Critical	High-spectral-resolution imaging spectroscopy of CO2, CH4 and O2 at 1-10 km spatial resolution with 0.1 to 0.5% accuracy.
1	B	CH4 Mole Fraction	Critical	High-spectral-resolution imaging spectroscopy of CO2, CH4 and O2 at 1-10 km spatial resolution with 0.1 to 0.5% accuracy.

CSQ ID	KAO ID	Geophysical Observable	Priority Level	Specification Text Summary
1	B	NO2 Mole Fraction	Critical	High-spectral-resolution imaging spectroscopy of NO2 and CO at 1-10 km spatial resolution
1	B	CO Mole Fraction	Critical	High-spectral-resolution imaging spectroscopy of NO2 and CO at 1-10 km spatial resolution
1	B	Fire radiative power	Supporting	High-spatial resolution (< 30m) multi-spectral and hyperspectral imaging and shortwave IR and thermal IR imaging (< 100m).
1	B	Fire fractional cover	Supporting	High-spatial resolution (< 30m) multi-spectral and hyperspectral imaging and shortwave IR and thermal IR imaging (< 100m).

Table 3: Example CSQ-KAO-Geophysical Observable mapping table for CSQ-1

This table was then imported into the project database which enables the connectivity to the mission, instrument, and measurement capability records contained in the CEOS Database. This connectivity has then been used to produce an initial capability gaps estimate for all the GO identified as critical and linked to a CEOS Database measurement. These initial gap analyses are provided as a stand-alone document, with an example shown in Appendix C.

3: High-level Capability Gap Analysis

In total, 870 mappings between CSQs, their KAOs, and Geophysical Observables were made. This constitutes a high-level binary gap analysis based on presence and absence of linkages between specified observables and instrument capabilities in the project database (D4).

CSQ	Question	# GO
CSQ-1	What anthropogenic and natural processes are driving the global carbon cycle?	28
CSQ-2	How has the land biosphere responded to human activity and climate change?	42
CSQ-3	How has the ocean carbon cycle responded to anthropogenic CO2 and climate change?	21
CSQ-5	What processes drive changes in sea level in the coastal ocean?	28
CSQ-7	How do coastal processes mediate exchanges between land, atmosphere and the open ocean?	59
CSQ-8	How are coastal areas contributing to the global carbon cycle, and how are they responding to climate change and human pressures?	78
CSQ-20	What are the key drivers for the mass balance change of the ice sheet, the ice shelves and the glaciers?	40
CSQ-21	What are the dominant physical processes that drive the sea ice thermo-dynamic state and variability	46
CSQ-24	Determine the relationship between changes in Polar regions and global climate variability?	15
CSQ-25	How does the cryosphere impact on Polar ecosystems, and how is the changing climate altering these feedbacks?	38
CSQ-33	How does the solid Earth deform under present and past ice loads and what does it tell us about its rheology?	21
CSQ-35	Can we quantify erosional processes of drainage basins and the resulting sediments discharge to the oceans	13

CSQ	Question	# GO
CSQ-36	Can we observe, model and forecast the deformation processes during the seismic cycle at plate boundaries, from pre- to post-seismic phases and during the inter-seismic phase ?	28
CSQ-38	How does Earth's crust evolve in interaction with internal geodynamic processes, and how does this reshape the Earth's surface over the long-term?	9
CSQ-43	What are the main coupling determinants between Earth's energy, water and carbon cycles? How accurately can we predict the forcings and feedbacks between the different components of the Earth system?	38
CSQ-44	How important are anthropogenic influences on the water cycle, and how accurately can we predict them?	32
CSQ-45	How can we reduce the uncertainties in the surface energy budget while improving the estimate of the internal flow within the climate system?"	61
CSQ-46	How does the Earth energy imbalance and Earth heat inventory changes over time and why? And what can we learn from this for the interplay between effective radiative climate forcing, Earth's surface temperature response and climate sensitivity, as well as	79
CSQ-48	How can we improve the monitoring and understanding of planetary heat exchange at regional scale? And which essential advancements can we achieve for research and monitoring on weather and climate patterns?	81
CSQ-51	What are the mechanisms that couple the lithosphere, atmosphere and ionosphere, and can they be modelled and monitored with adequate to support hazard risk management ?	22
CSQ-55	What are local patterns of ecosystem structure, composition and functions worldwide?	51
CSQ-56	Where and how are ecosystems undergoing critical transitions?	40
	Total	870

Table 4: CSQs and the number of Geophysical Observables

Of the 870 mappings, 411 of those were marked as priority 'critical'. The top 20 of these by count is shown in Table 5, with the full list of 'critical' Geophysical Observables shown in Appendix D.

Geophysical Observable ***CEOS DB, OSCAR Variables, or New indicated***	**Number**
CEOS: Gravity field	16
CEOS: Gravity gradients	11
CEOS: Ice sheet topography	11
CEOS: Land surface imagery	9
CEOS: Ocean chlorophyll concentration	9
CEOS: Land surface topography	8
CEOS: Atmospheric specific humidity (column/profile)	8
CEOS: Atmospheric temperature (column/profile)	8

Geophysical Observable *CEOS DB, OSCAR Variables, or New indicated*	Number
CEOS: Above Ground Biomass (AGB)	7
CEOS: Sea surface temperature	7
CEOS: Land surface temperature	6
CEOS: Ocean surface currents (vector)	6
CEOS: Ocean suspended sediment concentration	6
CEOS: Ocean temperature	6
CEOS: Chlorophyll Fluorescence from Vegetation on Land	6
CEOS: Vegetation Canopy (height)	6
CEOS: Sea Surface salinity	5
OSCAR: River discharge	5
New: Vegetation water content	5
CEOS: Coastal sea level (tide)	5

Table 5: Top 20 Geophysical Observable marked as priority 'critical' (full list in Appendix D)

In the Excel version of Deliverable 5, a matrix with counts of the number of Geophysical Observables per CSQ for priority critical GOs is included to support detailed analysis.

4: Capability Gap Analysis Based on Scientific Requirements

Three CSQs were selected for a deeper analysis based on scientific requirements in order to demonstrate examples of what the more detailed gap analysis process would look like, going beyond a simple presence/absence database search. The three science questions were chosen to represent different types of CSQ with a range of different observation requirements. These detailed gap analysis for these CSQs are outlined below, with references included in Appendix E.

4.1: CSQ-3: How has the ocean carbon cycle responded to anthropogenic CO_2 emissions and climate change?

4.1.1: Science Requirements

The ocean plays a key role in the global carbon cycle and climate by regulating the atmospheric concentrations of CO_2 and their changes over time. The ocean contains more than 60 times as much carbon as the atmosphere (c.f., DeVries 2022), and exchanges more than 90 billion tons of carbon (GtC) with the atmosphere each year. It also acts as an important "sink" for atmospheric carbon, absorbing a quarter of the 10.4 $GtCO_2$ carbon dioxide (CO_2) emitted by fossil fuel combustion and other human activities (Friedlingstein et al. 2023). The ocean carbon cycle has therefore been a key focus for Earth

observations (EO) for more than four decades. These measurements are now becoming more critical as the ocean composition, thermal structure and dynamics respond to climate change.

The amount of carbon that is exchanged between the ocean and the atmosphere is controlled by (i) the exchange across the interface (solubility pump), (ii) the uptake and release of carbon by photosynthesis and respiration (biological pump), and (iii) ocean dynamics, which continually exchanges water between the near surface and greater depths (Fig. 1). The exchange of CO_2 across the air-sea interface is regulated primarily by the ocean solubility pump, whose efficiency is governed by three mechanisms. The first is Henry's Law, which states that the amount of dissolved gas in a liquid is proportional to the partial pressure of the gas above the liquid. The flux of CO_2 through the ocean surface is therefore proportional to differences in the CO_2 partial pressure (pCO_2) across the air-sea interface. The second regulates the amount of CO_2 that can remain dissolved in seawater, which is inversely proportional to temperature (c.f., Woolf et al. 2016). Finally, the flux of carbon across the air-sea interface is modulated by mechanical mixing by waves and the resulting transport by air bubbles. Once atmospheric carbon has been transferred into the ocean, it's fate is controlled primarily by the so-called biological pump, which regulates ocean carbon content through photosynthesis, respiration and the precipitation of particulate organic carbon. The third process controlling the uptake of atmospheric CO_2 by the ocean is ocean dynamics, which continually replaces near-surface water with deep water, modifying the surface pCO_2, and thus the efficiency of the solubility pump.

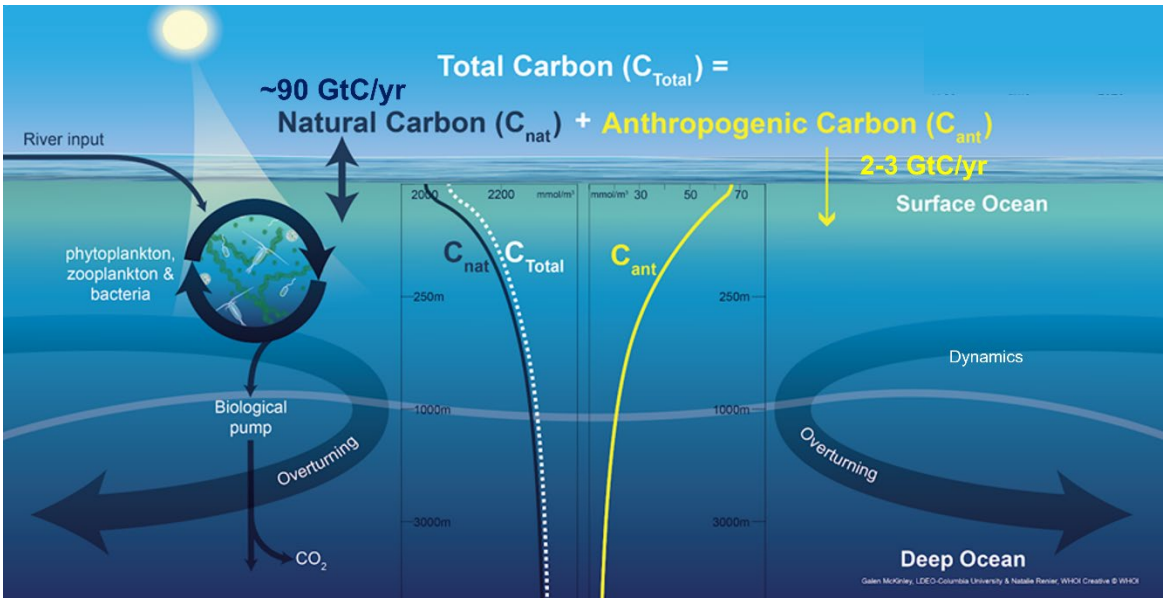

Fig. 1: Ocean carbon exchange processes. The total carbon (C_{Total}) includes contributions from the natural carbon (C_{nat}) and anthropogenic carbon (C_{ant}) cycles (from Crisp et al., 2022).

Space-based remote sensing observations are playing an increasingly important role in studies of the ocean carbon cycle, but these measurements must be combined with in situ measurements and models to describe ocean carbon stocks and fluxes. To date, space-based ocean carbon cycle observations have focused primarily on ocean colour, which provides key constraints on the ocean biological pump. These

measurements are now being collected by a growing fleet of purpose-built ocean colour and chlorophyll fluorescence sensors (c.f., Brewin et al., 2023). Other space-based observations have focused on sea surface temperature, ocean topography, ocean surface winds and salinity, which provide information about ocean dynamics. This suite of biological and physical observations is now providing key insights into both the ocean biology and transport, but provide much less direct insight into the exchange of CO_2 between the ocean and the atmosphere and thus, the efficiency of the ocean carbon sink.

The gap in measurements of direct ocean-atmosphere exchange is becoming increasingly policy-relevant as the nations of the world attempt to mitigate the effects of climate change by reducing greenhouse gas emissions and preserving and enhancing natural CO_2 sinks, such as the ocean. As noted above, the ocean sink is currently responsible for absorbing a quarter of all anthropogenic CO_2 emissions. However, there is growing uncertainty about how this sink has evolved over the past two decades and how it will continue to evolve as the ocean responds to ongoing human activity and climate change. Specifically, how will the ocean solubility pump and ocean dynamics respond to increasing atmospheric temperatures? How will the ocean's biological pump respond to increased temperatures and ocean acidification? Will the ocean sink efficiency be reduced as the ocean becomes more saturated with anthropogenic CO_2? How will the carbon flux between the land and ocean change in response to climate change? How will the ocean sink respond if anthropogenic emissions are substantially reduced? If anthropogenic CO_2 emissions are reduced to near zero, could the ocean sink reverse, such that the ocean becomes a source of CO_2? If the scientific community does not have the data needed to answer these questions, changes in the ocean sink efficiency could introduce confusion that could undermine sound emission reduction policies.

Improved, spatially-resolved measurements of vertical gradients in pCO_2 across the air-sea interface are needed to monitor ocean-atmosphere carbon fluxes on policy-relevant time-scales (c.f., Landschützer et al., 2020). Until recently, pCO_2 could only be measured using ship-based in situ sampling methods. These methods are accurate, but the measurements are extremely sparse, sampling only about 2% of the 1° x 1° grid boxes across the ocean at monthly intervals from 1982 to present. The sampling density of pCO_2 measurements has recently been increased by augmenting the ship-based measurements with in situ observations from BGC-Argo floats and other uncrewed surface vehicles (USVs) that can now measure pCO_2 with an uncertainty of ~2 µatm, which is comparable to ship-based observations.

These in situ measurements now provide a useful climatological constraint on the global ocean CO_2 uptake on multi-decadal time scales. For example, given the available pCO_2 measurements, both observation-based products and models show that the global ocean sink is increasing in response to increasing atmospheric CO_2 concentrations. However, these two methods indicate different rates of change, such that their sink estimates are diverging over time with models reporting a ~1 GtC/yr smaller sink than observation-based data-products (c.f., Hauck et al., 2020). A far denser and more frequent set of measurements is needed to monitor changes in the ocean sink on policy-relevant time scales.

In principle, high-resolution, global space-based measurements could provide the spatial and temporal sampling needed to dramatically improve our understanding of surface ocean of CO_2 fluxes and their implications for the evolution of the ocean sink. While there is currently no known way to estimate sub-

surface pCO_2 using space-based remote sensing methods, it is possible to measure atmospheric pCO_2. Spatially-resolved high-resolution spectroscopic measurements of reflected sunlight can be analysed to yield estimates of the atmospheric CO_2 dry air mole fraction (XCO_2) with precisions and accuracies better than 0.25% (~1 part per million, ppm, out of the 420 ppm background). These spatially-resolved XCO_2 fields can be analysed with atmospheric inverse models to yield estimates of surface-atmosphere CO_2 fluxes with uncertainties in the range of 0.1 to 1 kg of CO_2 per square metre per year ($kgCO_2/m^2/yr$) on spatial scales as fine as 1° x 1° (c.f., Byrne et al., 2022). While this is not yet adequate to constrain air-sea fluxes over the open ocean, these measurements could be optimised to meet this need.

4.1.2: Measurement Requirements for Ocean Fluxes

To quantity the atmospheric CO_2 anomalies associated with ocean-atmosphere CO_2 fluxes, we need space-based XCO_2 estimates with even higher precision and accuracy. Anthropogenic CO_2 emissions or intense natural terrestrial sinks, such a forests, can produce fluxes exceeding 1 $kgC/m^2/yr$, yielding XCO_2 anomalies as large as several parts per million (ppm) on spatial scales of 1° x 1° (c.f., Byrne et al, 2022; Friedlingstein et al. 2023). In contrast, even the most intense ocean fluxes and their associated XCO_2 anomalies are typically 10 to 100 times smaller (~0.1 ppm) on these spatial scales. So, while space-based measurements of XCO_2 with precisions and accuracies of 0.5 to 1 ppm are now providing important insights into anthropogenic emissions and the land carbon cycle, they do not provide the sensitivity needed to quantify ocean fluxes.

This is a critical limitation on current space-based XCO_2 sensors, but it is not a show stopper. The first generation of space-based XCO_2 sensors, including Japan's GOSAT and GOSAT-2 and NASA's OCO-2, and OCO-3, were optimised for quantifying XCO_2 to 1 ppm on regional scales (10°x10°). The next generation, including GOSAT-GW and CO2M were optimised to constrain anthropogenic emissions from point sources and large urban areas, and thus yield XCO_2 precisions and accuracies of 0.5 to 1 ppm on spatial scales as small as four square km. These systems are not optimised to constrain ocean CO_2 fluxes.

While substantially higher measurement precision and accuracy is required to quantify XCO_2 anomalies and fluxes over the open ocean, much lower spatial resolution is needed for this application. Air-sea CO_2 flux estimates with accuracies of 20% on spatial scales of 1° x 1° at monthly intervals could revolutionise our understanding of ocean carbon fluxes and the evolution of the ocean sink. This goal is not that far from our current capability. For example, OCO-2 typically yields single-sounding random errors of ~0.5 ppm when observing ocean glint, and collects ~400 soundings per degree of latitude. These soundings can be screened for clouds and then co-added to yield XCO_2 estimates with negligible random error at 1° resolution along the OCO-2 ground track. However, random errors are not the obstacle that must be overcome to produce useful estimates of ocean CO_2 fluxes. The need to reduce systematic measurement biases to << 0.1 ppm is a substantially more challenging problem. To achieve that goal, the instrument calibration, retrieval algorithm and data product validation approaches must be substantially improved.

Lessons learned from the OCO and GOSAT missions have provided substantial insight into both pre-launch and on-orbit calibration methods (c.f., Kuze et al., 2016; Kataoka et al., 2017; Lee et al., 2017; Keller et

al., 2022). These lessons must be incorporated into sensor designs and calibration methods to build sensors that are sufficiently well calibrated and stable to yield estimates of XCO_2 with systematic errors <0.1%. Retrieval algorithm accuracy has increased steadily through the GOSAT and OCO missions (c.f., O'Dell et al, 2018), and is expected to continue improving as more accurate laboratory measurements of CO_2, O_2, and other gases become available and other algorithm refinements are implemented. Additional progress in this area is also needed to yield nearly bias-free XCO_2 estimates over the ocean.

Perhaps the most challenging advance needed is in the area of ground-based validation of the XCO_2 data products. To validate their XCO_2 estimates, the GOSAT and OCO teams have adopted a comprehensive validation protocol that uses simultaneous upward-looking and downward-looking measurements over Total Carbon Column Observing Network (TCCON) stations as a transfer standard between the space-based measurements and the WMO in situ standard (Wunch et al., 2011; 2017). Additional information about the vertical profile of CO_2 can be obtained from in situ measurements from balloon-borne AirCore sensors (Karion et al., 2010; Membrive et al., 2017). This validation approach could be extended to yield further improvements in XCO_2 accuracy by expanding the number of TCCON and AirCore stations in marine environments to more reliably identify and correct biases in XCO_2 estimates over the ocean. In addition, XCO_2 profiles collected by low-altitude (< 6 km) aircraft will be needed to validate flux estimates (c.f., Byrne et al., 2022). Fortunately, this expanded XCO_2 and flux validation system can be implemented for a small fraction of the cost of a space-based sensor.

4.1.3: Capabilities of Existing and Planned Missions

Brewin et al., (2022) provide a comprehensive review of existing and planned satellite sensors for monitoring the ocean carbon cycle from space. They describe the current state of the art, identify measurement and modelling gaps and near-term opportunities for space-based observations of primary production (PP), particulate organic carbon (POC), phytoplankton carbon (C-phyto), dissolved organic carbon (DOC), inorganic carbon (IC), and cross-cutting themes (e.g., Blue carbon (BC), extreme events (EE), carbon budget closure). The vast majority of the missions catalogued in this review use hyperspectral imagers to monitor ocean colour, with a range of spatial and temporal sampling frequencies. These missions include the Plankton, Aerosol, Cloud, ocean Ecosystem (PACE) mission, Geosynchronous Littoral Imaging and Monitoring Radiometer (GLIMR), Environmental Mapping and Analysis Program (EnMAP), FLuorescence Explorer (FLEX), Sentinel-4 (S-4), Sentinel-5 (S-5), Surface Biology and Geology (SBG) mission and MetOp-SG Multi-Viewing Multi-Channel Multi-Polarisation Imaging (3MI) instrument. While these space-based sensors are increasingly important for global studies of the ocean biosphere and biological pump, they provide no direct constraints of the flux of CO_2 across the ocean-atmosphere interface.

The CEOS Database lists a large suite of space-based instruments designed to monitor ocean physical and chemical properties that are essential for modelling ocean transport. These include sensors for monitoring sea surface temperature (46 instruments), surface salinity (3 instruments), ocean dynamic topography (12 instruments), wind speed (31 instruments), ocean vector winds (11 instruments) and other variables. The measurements collected by these instruments are critical for understanding the impact of ocean dynamics on the ocean carbon cycle, but none provide quantitative constraints on ocean surface fluxes of CO_2.

In addition, the CEOS Database lists 44 missions that can measure the atmospheric CO_2 mole fraction. These missions can be organised into three classes (c.f., CEOS EOHandbook, https://database.eohandbook.com/ghg/): (i) Global GHG mappers, (ii) facility scale plume monitors, and (iii) operational meteorological sounders. Of these classes, the global GHG mappers are best suited for quantifying surface-atmosphere CO_2 fluxes from weak, spatially-extended natural sources and sinks.

The first generation of global GHG mappers includes Japan's GOSAT and GOSAT-2 and NASA's OCO-2 and OCO-3, missions. These sensors were designed to demonstrate that high spectral resolution, space-based measurements of reflected sunlight could yield XCO_2 and XCH_4 estimates with precisions and accuracies of < 0.25% (1 ppm CO_2, 4 ppb CH_4) on regional scales (10° x 10°). These objectives were accomplished by combining sensitive, high-resolution spectrometers (c.f., Kuze et al., Crisp et al., 2017) with rigorous calibration systems, continuously improving XCO_2 retrieval algorithms, expanding data product validation systems and rapidly-evolving atmospheric CO_2 flux inversion models. OCO-2 and OCO-3 have substantially exceeded their measurement requirements, demonstrating XCO_2 estimates with root mean squared errors (RMSEs) of approximately 0.8 ppm and 0.9 ppm, respectively, on spatial scales as fine as ~2 km^2 (Taylor et al., 2023). While these results are now providing new constraints on CO_2 emissions from anthropogenic activities and new insights into CO_2 sources and sinks in the terrestrial carbon cycle, small systematic errors (< 0.5 ppm) in the XCO_2 estimates acquired over the ocean have precluded their use for estimating CO_2 fluxes through the air-sea interface (c.f., Byrne et al., 2022).

The second generation of global GHG mappers, including Japan's GOSAT-GW and the Copernicus CO2M constellation, are optimised for increased spatial coverage and resolution. For example, unlike OCO-2, which samples only 7% of the globe each month, the CO2M constellation will sample the globe at weekly intervals at a spatial resolution of ~4 km^2, with single-sounding accuracies < 0.7 ppm (CO2M MRD, 2020). With their greater spatial coverage, these sensors are expected to yield far more information about anthropogenic emissions from localised sources such as large fossil fuel-fired power plants and large urban areas. However, their instrument designs were not optimised to yield XCO_2 estimates with the precision and accuracy needed to yield useful constraints on CO_2 fluxes over the ocean (< 0.1 ppm) and their mission architectures are optimised to maximise the spatial resolution and coverage over land, with more limited observations of ocean glint.

More recently, these purpose-built, global GHG mappers have been joined by a growing number of high-spatial resolution imaging sensors that can detect the most intense CH_4 and CO_2 emissions plumes. These facility-level plume monitors include private-sector missions such as GHGSat and MethaneSAT, public-sector missions such as PRISMA, EnMAP, and EMIT and hybrid public-private partnerships, such as Carbon Mapper. These sensors can sample only a fraction of the globe, but exploit their high spatial resolution (30-50 m) to detect and quantify intense emission plumes associated with methane extraction, transport and use, and CO_2 plumes from the largest fossil fuel fired power plants. They have no sensitivity to the much weaker, but more spatially extensive CO_2 or CH_4 fluxes from the ocean.

The third class of CO_2 missions listed in the CEOS Database includes operational meteorological sounders, such as NASA's AIRS, NOAA NPP CrIS, and Metop IASI. These instruments collect spectra within CO_2 bands

at thermal infrared wavelengths to retrieve atmospheric temperature profiles. These observations are sensitive to CO_2 mole fractions at altitudes above the middle troposphere (~5 km), but have very little sensitivity to CO_2 concentrations near the surface. They are therefore not well suited to monitoring surface-atmosphere CO_2 fluxes.

In summary, while there is a growing fleet of space-based sensors designed to monitor properties critical to our understanding of the ocean carbon cycle and its changes over time, none have the precision or accuracy needed to provide useful quantitative constraints on the flux of CO_2 across the air-sea interface.

4.1.4: Capability Gaps and Prospects for Filling These Gaps

Sensors that are optimised to deliver highly precise and accurate XCO_2 estimates over the ocean have not yet been demonstrated. No new technologies should be needed for these sensors, but they must be designed to maximise precision, accuracy, and calibration stability, perhaps while sacrificing some spatial resolution and coverage, since these are less critical for monitoring fluxes over at least the open ocean. These purpose-built ocean flux sensors should also be better optimised to observe reflected sunlight from the bright ocean glint, which will provide the highest possible signal to noise ratios and thus the highest sensitivity to the weak CO_2 anomalies associated with ocean fluxes. Lessons learned during the development of the first two generations of GHG sensors should provide the information needed to maximise calibration accuracy and stability. These sensors should also be integrated into payloads that include other sensors designed to identify sources of bias that could introduce systematic errors in XCO_2 or CO_2 flux. For example, contamination by optically thin clouds and aerosols are often the largest sources of error for XCO_2 sensors. Uncertainties in the degree of polarisation can also introduce systematic biases in ocean glint measurements. Compact, low-mass cloud and aerosol sensors, like those adopted for the CO2M constellation could address many of these issues.

Perhaps the most substantial limitation of these first- and second-generation space-based GHG sensors is the lack of a ground-based validation system that can identify and characterise sources of bias over the ocean. Comparisons of XCO_2 estimates derived from GOSAT and OCO observations to TCCON and AirCore measurements have played a major role in the identification and correction of systematic XCO2 estimates over land.

To enable such improvements over the ocean, the TCCON and AirCore networks would have to be expanded in locations characterising marine environments. Currently, there are no direct methods for validating CO_2 fluxes derived from space-based XCO_2 estimates on spatial scales of 1° to 10°. The best available indirect approach employs comparisons of the a posteriori CO_2 fields derived by the flux inversion models to near-surface vertical profiles of CO_2 collected by in situ sensors carried aloft by fixed-wing aircraft or balloons (c.f., Byrne et al., 2022). This approach has provided useful insights into flux inversion model errors over continental sites, but has not yet been used widely over the ocean. The one exception is the limited use of vertical profiles collected from NASA's Atmospheric Tomography (ATom) mission over the ocean. These measurements clearly show biases in the OCO-2 XCO_2 products, but were not extensive enough to validate fluxes derived from the products.

Currently, only four TCCON stations sample predominately marine environments (Ascension, Reunion, Darwin and Burgos), and each of these stations faces logistical challenges that sometimes compromise their data quality or latency. Additional support for these stations along with additional stations that cover a broader range of latitudes are needed to deliver the levels of accuracy needed to quantify ocean fluxes. There are currently no AirCore sites near coastlines because balloons carry these systems to ~25 km altitude and then release them for an unguided descent on parachute. The sensor package must then be retrieved quickly (before the sample starts mixing) to record their results. If deployed near coastlines, small uncertainties in wind speed or direction could cause the sensor packages to be lost at sea, along with their data. Fortunately, groups at the NOAA Global Monitoring Laboratory, and at MeteoSuisse are developing autonomous gliders that can return the AirCore sensor packages to a specified location. Once these gliders are available, it should possible to deploy AirCore packages from shorelines or even ships.

4.1.5: Conclusions

Space-based measurements are now providing critical insights into ocean dynamics, biogeochemistry and blue carbon. However, they are providing little quantitative information about the exchange of CO_2 between the ocean and the atmosphere, or evolution of the critical ocean CO_2 sink, which is currently responsible for absorbing more than a quarter of all anthropogenic emissions. To address this growing measurement gap, we need to augment the existing in situ measurements of pCO_2 with high-resolution (1° x 1°), global, space-based constraints on the fluxes of CO_2 across the air-sea interface.

Existing and planned space-based GHG sensors are now providing new insights into anthropogenic emissions and carbon fluxes from the land biosphere, but do not have the sensitivity to measure the much weaker, but more spatially-extensive ocean CO_2 fluxes because they have not been optimised for that application. Purpose-built, space-based ocean CO_2 sensors with these capabilities require no new technologies, but will need updated sensor designs and mission architectures optimised for this application. They will also require expanded ground-based and airborne validation systems to identify and correct systematic biases in the space-based observations.

4.2: CSQ-20: What are the key drivers of change in mass balance of the ice sheet, ice shelves and glaciers?

4.2.1: Science Requirements

Fluctuations in Earth's ice mass have occurred in almost all regions of the cryosphere, in response to change in environmental forcing mechanisms and as a longer-term response to climate change. Satellite observations have shown that the mass balance of the Antarctic and Greenland Ice Sheets has changed dramatically over the last 40-years, with ice loss increasing by six times over this period, increasing global sea levels by 17.8 mm (Shepherd et al., 2018). If these rates continue, ice sheets are expected to raise sea levels by a further 17 cm – exposing an additional 16 million people to annual coastal flooding by the end of the century (Slater et al., 2020).

In the ice sheet margins satellite altimetry has measured rapid lowering of the ice surface (Shepherd et al., 2019), with rates of up to 9 m/yr observed on Smith Glacier in West Antarctica (McMillan et al, 2014). In many regions where surface lowering has been observed ice velocity measurements (Rignot et al., 2011) have shown that the flow of ice is also speeding up, with long term increases in ice speed of over 42% observed on Pine Island Glacier in West Antarctica (Mouginot et al, 2014). While in Greenland surface melt driven lubrication drives the majority of ice mass loss, in Antarctica ocean water drives melt, demonstrating that the dominant physical process is different in the North and South Hemispheres.

Ice dynamics, which relates to the change in the rate of ice flow, is responsible for approximately one third of all ice mass loss on the Greenland Ice Sheet, and almost all (98%) ice mass loss on the Antarctic Ice Sheet (Slater et al., 2020). Ice dynamic change is primarily concentrated in the marine terminating regions of the ice sheets, which are often also grounded below present-day sea level. IPCC reports consistently state that the largest remaining uncertainty in the ice sheet contribution to sea level rise is linked to ice dynamics, where the speedup of glaciers can lead to imbalance and then instability, through the Marine Ice Sheet Instability (MISI) and Marine Ice Cliff Instability (MICI) mechanisms. In Antarctica ice dynamics are thought to be largely driven by incursions of warm, deep circumpolar water onto the continental shelf, which causes enhanced melt (Dutrieux et al., 2014; Jenkins et al., 2018). More recently, the very high temporal resolution (weekly) satellite observations from operational ESA-EC missions such as Sentinel-1a and -1b, have enabled short-term, seasonal changes in ice speed the be better characterised on the Greenland Ice sheet, and observed for the first time in Antarctica (Wallis et al., 2023). This enables short-term ice dynamics to be studied in more depth, providing further insight on the speed with which changes in ice speed can occur, and enabling us to better understand the physical processes driving this change in different regions of the world.

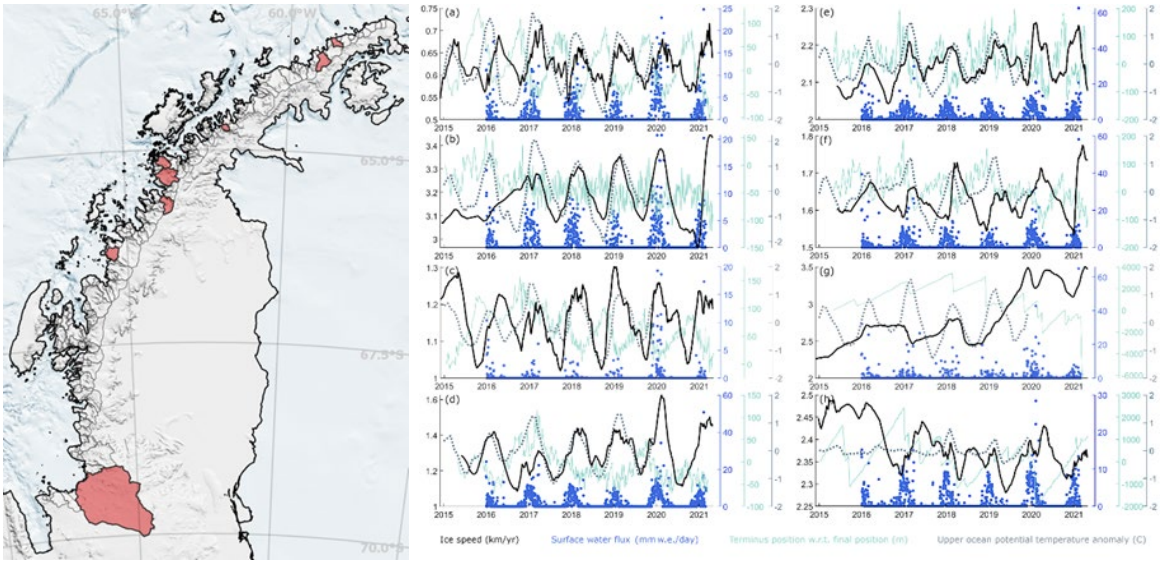

Figure 3: Highlight glaciers' time series of ice speed, surface water flux, terminus position and ocean temperature anomaly. a–h, Time series of Kalman-smoothed ice speed (black solid line), RACMO2.3p2 surface water flux (snowmelt plus rain; blue dots)43,52, terminus position with respect to the final

position (green solid line) and upper-ocean (110 m) potential temperature anomaly (grey dashed line)56. Time series are shown for unnamed north Bone Bay (a), Gavin Ice Piedmont (b), Leonardo (c), Hotine (d), Trooz (e), Keith (f), Cadman (g) and Fleming (h) Glaciers. Highlight glaciers in a–f were selected based on their large seasonal ice speed variability (autocorrelation values of 0.648, 0.314, 0.586, 0.703, 0.575 and 0.575, respectively), to give a spread of locations along the west AP, and to show a range of faster and slower mean ice speeds. w.r.t., with respect to; w.e., water equivalent. From Wallis et al., 2023.

While the ice sheets contribute one third of the total sea level rise budget, ice loss is also occurring on mountain glaciers and ice caps (Paul et al., 2015). Observations have shown that glacier mass loss has increased from -120 Gt per year in the 1970 to -327 Gt per year between 2010 and 2019. In mountain glacier regions the dominant cause of ice loss is increasing air temperatures (Slater et al., 2021). Studies should quantify the regional variability in the change in ice mass of different elements of the cryosphere, such as the glaciers, ice sheets and ice shelves, and understand the physical mechanisms driving this change.

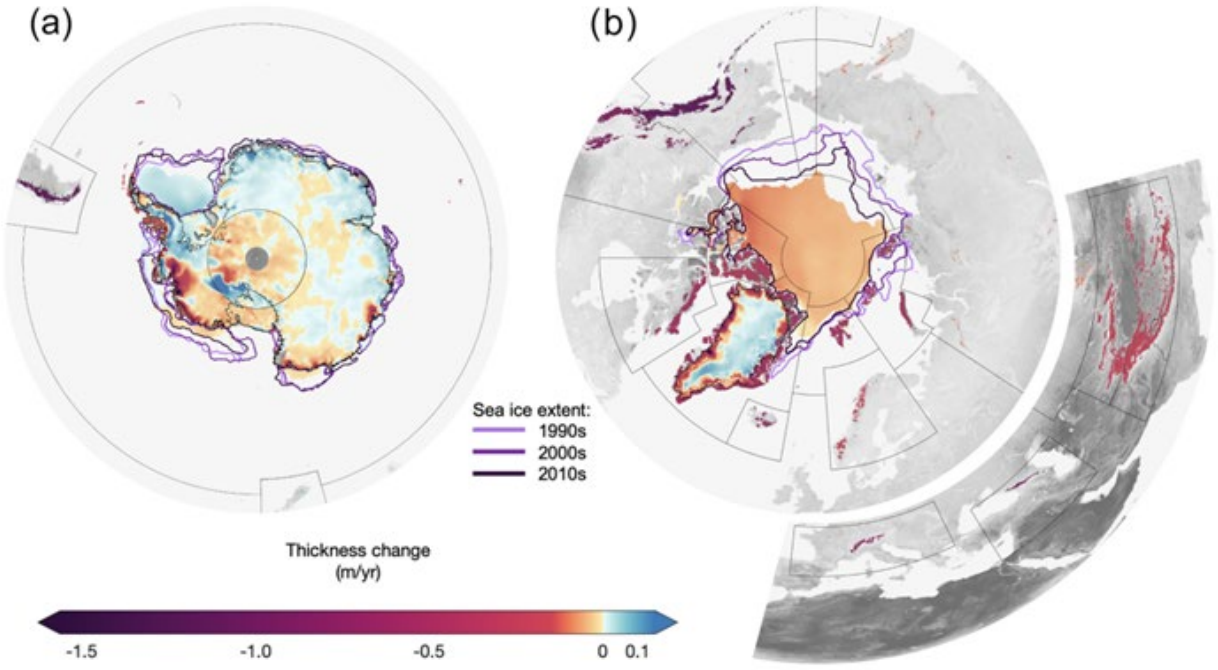

Figure 4: Average rate of ice thickness change in the (a) Southern Hemisphere and (b) Northern Hemisphere. Changes in Antarctic (1992– 2017) and Greenland ice sheet (1992–2018) thickness were estimated using repeat satellite altimetry following the methods of Shepherd et al. (2019). Sea ice thickness trends between 1990 and 2019 are determined from numerical sea ice and ocean modelling (Zhang and Rothrock, 2003), as well as the average minimum of sea ice extent in February (Antarctic) and September (Arctic) (purple lines) for each decade during the same period. Glacier thickness change between 1992 and 2018 for glacier regions defined in the Randolph Glacier Inventory (RGI Consortium, 2017) (black boundaries) are from mass change estimates (Braun et al., 2019; Foresta et al., 2016; Jakob

et al., 2020; Tepes et al., 2021; Wouters et al., 2019; Zemp et al., 2019b) which have been converted to a thickness change assuming an ice density of 850 kg m−3. From Slater et al., 2021.

Ice Shelves are regions of meteoric ice that has flowed from the ice sheet out over the ocean (Cook and Vaughan, 2010). When ice mass is lost from ice shelves it does not directly contribute to sea level rise as the ice is already in hydrostatic equilibrium with the ocean. However, ice shelves do provide resistive force to the grounded ice sheet that they buttress thereby indirectly contributing to global sea level rise when they are lost (Rott et al., 1996; Rignot et al., 2004). More directly, mass loss from both ice shelves and the ice sheet leads to increased freshwater flux into the Polar oceans, impacting deep water formation and hence the major shallow and deep ocean circulation pathways between the Arctic and Southern oceans (Davison et al., 2023). While most aspects of the mean circulation and structure are well described quantitatively, variability is much less well characterised. This connectivity of the global oceans gives the remotest Polar regions a global reach and ensures their wider impact on Earth's systems.

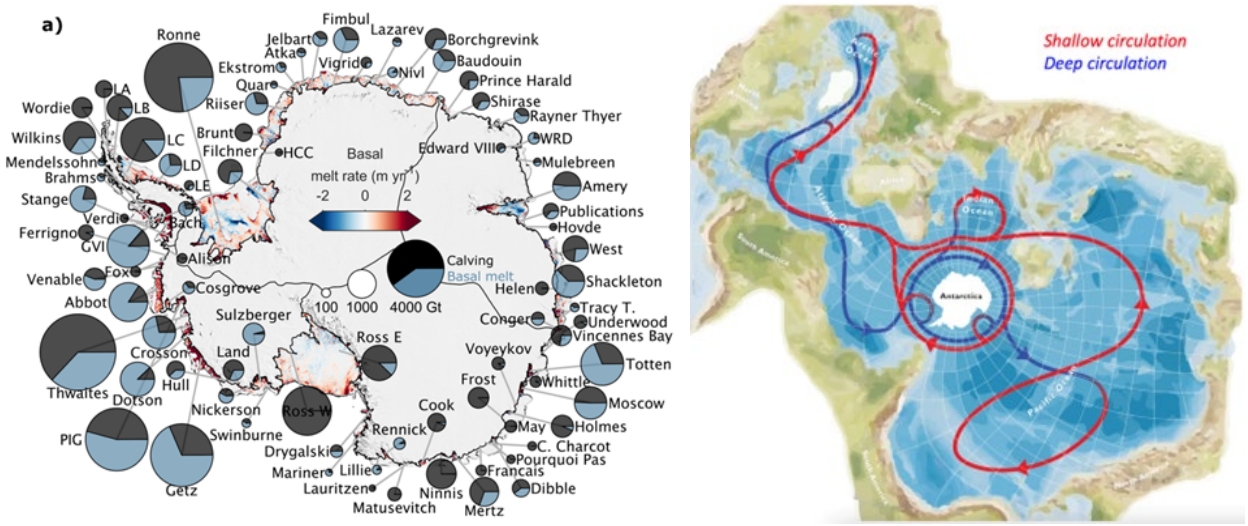

Figure 5: a) Total liquid and solid freshwater flux from Antarctic Ice shelves from 1997 to 2021 (Davison et al,. 2023). b) Ocean circulation pathways.

High-frequency, high-spatial resolution satellite measurements are required over all components of the cryosphere in order to provide the global coverage and temporal sampling required to monitor change. Measurements of these essential climate variables are required to dramatically improve our knowledge of the physical processes driving change and to characterise the different modes of variability across the cryosphere system. Satellite observations have shown that present day ice mass loss is tracking the high-end IPCC future climate scenarios (Slater et al 2021). While studies show that this contribution is projected to be larger in the future, the size of this contribution is uncertain. Measurements of present day change

are essential in order to more accurately predict future evolution of ice mass change (Cornford et al., 2015), and this knowledge will be used to inform government policy and planning on sea level rise.

4.2.2: Measurement Requirements

In order to monitor mass change of the cryosphere, satellite observations are required over all glaciers and ice caps which are distributed globally, and the Antarctic and Greenland Ice Sheets and Ice Shelves. A range of different satellite observations are required including measurements of change in ice speed (Joughin et al., 2008; Mouginot et al., 2014), surface elevation change (Shepherd et al., 2019), ice shelf basal melt (Davison et al., 2023), iceberg calving (Hogg and Gudmundsson., 2017), grounding line location and surface mass balance (van Wessem et al., 2018), which includes both precipitation and surface melt. We have established methods for remotely observing almost all of these parameters, with the exception of precipitation, however, effort must be invested in reducing the measurement error and uncertainty of all variables. Temporal sampling for these observations must be frequent enough to measure the known short and long-term variability, for example weekly measurements are required to accurately measure seasonal ice speed change (Wallis et al., 2023); and to characterise new modes of variability that haven't yet been detected. Uncertainty must be low enough to distinguish real geophysical change from background noise, and to measure change on small spatial scales. For example, high-spatial resolution (100's of metres) observations of change in both surface elevation and ice speed are required in the ice sheet margins and on smaller ~1 km wide glaciers, in addition to coarser spatial resolution (km scale) observations over the whole continental ice sheet. Measurements from a number of these glaciological variables can be combined to produce important higher-level datasets. For example, by combining information on ice speed with ice thickness, and knowledge on snowfall input into the basin, we can calculate ice sheet and glacier mass balance and therefore its sea level contribution (Shepherd et al., 2018). By partitioning mass loss into its constituent components we can understand the processes driving change, and learn about the environmental forcing mechanisms and how they impact on the cryosphere (Slater et al., 2020; Davison et al., 2023b). Overall, producing these datasets from satellite observations is a big data challenge which requires large remote storage capacity and High Performance Computer (HPC) facilities for the processing effort. New glaciological parameters are already being produced by exploiting advanced computer techniques to automate the production of historically manually intensive parameters such as calving front location (Surawy-Stepney et al., 2023) and grounding line position.

4.2.3: Capabilities of Existing and Planned Missions

C-band Synthetic Aperture Radar (SAR) satellites such as ERS-1/2 historically, and Sentinel-1 currently, are used to measure change in ice speed and the grounding line location. Ice speed measurements are primarily made using the intensity feature tracking technique which only requires amplitude information from SAR images (Strozzi et al., 2002), however coherent feature tracking (which also uses the phase component of SAR images), is used to make accurate measurements of ice speed in the slower flowing ice sheet interior where surface features are sparser. The differential interferometry technique is used to measure the ice sheet grounding line location and this requires both the phase and amplitude information of at least 3 SAR image pairs with a sufficiently short temporal baseline. In addition to the ESA mission C-

band SAR datasets, ice speed and grounding line measurements can be produced from CSA's C-band RADARSAT Constellation Mission; X-band SAR data acquired by DLR's TerraSAR-X, TanDEM-X and ASI's COSMO-SkyMed; L-band data from Jaxa's ALOS-PALSAR and future ESA mission ROSE-L and future NASA NISAR mission. The different radar frequencies (i.e. X-, C- L-band) of the SAR satellite missions have different penetration depths into the ice and snow surface, the depth of which is largely controlled by the density of the snowpack. Single frequency SAR datasets are also affected by a change in scattering horizon caused by the impact of weather and climate on the snowpack, for example, when surface melt occurs over a previously dry snow region. This vertical change in the scattering horizon can induce a horizontal artefact on ice speed measurements, and as multi-frequency SAR data from different satellite missions is co-temporaneously acquired, characterising both the magnitude and extent of these differences will become more important in the future. Ice speed measurements from SAR can be complimented by observations from multispectral optical instruments such as Landsat and Sentinel-2, however optical instruments are limited to summer-time-only measurements due to the absence of sunlight in the Polar regions during the winter months.

Ice sheet surface elevation change and ice shelf basal melt rates are measured using altimetry datasets (McMillan et al., 2014; Shepherd et al., 2019). ESA radar altimeters including ERS-1/2, ENVISAT, CryoSat-2 and Sentinel-3 provide a long-term (~40-year) continuous record of change, with near complete coverage over the whole ice sheet. High spatial resolution (500 metres) measurements are required in the ice sheet margins to properly capture the spatial pattern of change, and this can be achieved with swath processing of CryoSat-2 SARIn mode data (Gourmelen et al., 2018). This imaging mode is only available in the ice sheet margins and over mountain glaciers and ice caps, with radar altimetry measurements made in the lower resolution (km scale) LRM mode in the ice sheet interior. Swath processing of SARIn mode radar altimetry data could be applied across the whole ice sheet if future ESA missions such as CRISTAL are designed to operate in SARIn mode over those regions, which would increase the spatial resolution of the surface elevation data products. Radar altimetry struggles to retrieve high quality data in very mountainous terrain, such as the Himalayas and the Antarctic Peninsula, so spatial coverage is poorer in these regions. Swath mode data processing addresses this issue to some extent, but further work is required to improve elevation change retrievals over mountainous terrain. Beyond ESA altimetry missions, radar altimetry data is also acquired by the Ka-band CNES AltiKa satellite mission, and laser altimetry data is acquired by the NASA ICESat (2003 to 2009) and ICESat-2 (2018 to present) missions. Differences between altimetry mission frequencies (i.e. Ka vs Ku-band, and laser and radar altimetry), can be used to interrogate snow properties using the varying penetration depths of these different instruments.

4.2.4: Capability Gaps and Prospects for Filling Them

Sentinel-1b is no-longer operating and Sentinel-1a is now in poor health, therefore there is a substantial risk of an ESA C-band SAR data gap if Sentinel-1c is not launched in time. ESA and the EC should aim to launch Sentinel-1d at the earliest opportunity following the launch of Sentinel-1c to ensure a return to the 6-day repeat period which is so important for monitoring of the Polar regions. CryoSat-2 has exceeded its mission lifetime therefore there is a risk that SARIn mode capability will be lost if the CRISTAL mission is not launched before the CryoSat-2 mission ends.

In order to maintain phase coherence between SAR image pairs, a short temporal baseline is required as changes in the snow surface, either from fast ice flow (1 km/yr plus) or surface melt and snowfall, lead to incoherence. Weather events that affect the snow surface can occur on hourly timescales, and the most rapidly flowing ice streams (e.g. Pine Island Glacier flows at just over 4 km./yr) will displace and deform substantially over a matter of days. InSAR coherence at C-band can usually be maintained over the majority of the ice sheet if the SAR repeat period is 3-days or less, and this time period can be lengthened if the wavelength of the SAR dataset is longer, e.g. L-band acquisitions retain coherence for longer than shorter wavelength X-band sensors. InSAR coherence is not maintained over fast flowing ice streams, such as those found in West Antarctica and Jakobshavn Isbrae in Greenland over the 6-day Sentinel-1a/b repeat period, and even less of the ice sheet retains interferometric coherence over the 12-day temporal baseline when Sentinel-1 only has a single satellite in operation. Consequently, there is currently an observational gap for coherent SAR techniques over a substantial part of the Antarctic and Greenland Ice Sheets.

With all altimetry and SAR satellite missions there is an observational gap over the pole hole at high latitudes in Antarctica. The size of this hole varies according to the orbit used for different missions, and minimising the size of this data gap is always important for Polar monitoring. The observational gap at the pole hole is particularly large for the Sentinel-1 mission and is smallest for the CryoSat-2 radar altimetry mission. In the past the SAR pole hole data gap has been filled by rotating the RADARSAT satellite 180 degrees from its normal field of view to image the interior region only, but this major manoeuvre is risky and cannot be carried out regularly.

Gravimetry is the third of the independent mass balance measurement techniques, with this data largely acquired by the NASA-DLR Gravity Recovery And Climate Experiment (GRACE) satellite mission between 2002 and 2017 and then the GRACE follow-on mission from 2018 to present. GRACE gravimetry measurements have a coarse spatial resolution in comparison to cotemporaneous SAR and altimetry measurements, however, in the future finer spatial resolution will emerge from the ESA-NASA Mass-Change and Geosciences International Constellation (MAGIC) mission. While the improved spatial resolution of the MAGIC mission will still have some constraints, such gravimetry-based mass change observations will also yield a way to compare to and assess the corresponding sum of measurements of change in ice speed, surface elevation, ice shelf basal melt, iceberg calving, grounding line location and surface mass balance including precipitation and surface melt inverted to mass flux into the ocean, and their corresponding sea level rise contribution.

In-situ and airborne validation datasets are incredibly sparse, both spatially across ice sheets and glaciers, but even more so in terms of temporal sampling. Modes of temporal variability are much less well characterised than the spatial picture of change, and the timing of this change is critical for linking cause and effect with the driving physical processes. Absence of adequate validation data also limits our ability to better characterise the uncertainty of satellite measurements, therefore investment must be made in collecting this complimentary campaign data, both for existing data products, and the novel future datasets that we must seek to develop. The instruments required for these validation activities can in some cases be bought off the shelf, for example GPS sensors or in-situ interferometers for ice speed measurements, or can be built to specification if commissioned (e.g Ka- and ku-band airborne altimeters), so there the main barrier to collecting these validation datasets is investment in the instruments and

campaigns, rather than the technology readiness of the instrumentation. Due to the extreme weather and logistical constraints, there are substantially fewer validation datasets acquired in the Polar winter, when glaciological conditions and processes are different, therefore effort should be made to fill this gap.

The cryosphere is now changing so rapidly that the impact of extreme weather events can be seen in our traditional EO methods (Siegert et al., 2023), and may impact our ability to make high quality measurements of these important parameters in the future. For example, the extreme surface melt event over the Greenland Ice Sheet between the May–June and August–September 2012 caused a clear positive increase of approximately 0.5 m over the ice sheet surface elevation in the dry snow zone (ice sheet interior), as measured by the CryoSat-2 radar altimeter (Nilsson et al., 2015). This apparent increase in the ice sheet surface was actually caused by a change in the radar penetration depth and was therefore a measurement artefact that needed to be corrected, rather than representing real geophysical change. New datasets and algorithms may be required to make these essential measurements of the Polar regions in the future.

4.3: CSQ-56: Where and how are ecosystems undergoing critical transitions?

4.3.1: Review of the science requirements for the geophysical observables

Land ecosystems are complex systems of interconnected species and the physical environment. They have an integral role in the Earth's system. For instance, in terms of the global carbon cycle, the land CO_2 sink was 3.3±0.8 Gt C yr−1 during the 2013–2022 decade, about 31 % of total CO_2 emissions (Friedlingstein et al., 2023). However, there are major known sources of uncertainties when quantifying this figure, such as the responses of vegetation to variability in temperature and rainfall with particularly larger uncertainties in the tropics (Cox et al., 2013; Jung et al., 2017; Humprey et al. 2021) and tree mortality (Brienen et al., 2020; Hubau et al., 2020). These known sources of uncertainties in each component of the global carbon budget, defined as input data or processes, have a demonstrated effect of at least ±0.3 Gt C yr−1 (Friedlingstein et al., 2023). In terms of energy balance, forests have a net cooling effect from evapotranspiration that contributes to stabilise Earth's climate, for instance the Amazon contributes up to 50% of rainfall in the region and is crucial for moisture supply across South America (Staal et al., 2018).

Ecosystems critical transitions are characterised by i) the occurrence of alternative regimes under same environmental conditions and ii) by abrupt discontinuous transitions between regimes when a critical threshold is exceeded (Gsell et al., 2016). Fundamental changes at ecosystem level affect ecological processes and ultimately ecosystem services. Hence, reliable, consistent and systematic observations and tools for assessing ecosystem resilience and dynamics are required.

The systematic monitoring of ecosystem dynamics has been demonstrated using remote sensing time series across a range of ecosystem and change types (IPBES, 2019, Skidmore et al., 2021). With satellite-based sensors like Landsat and Sentinels 1 and 2 and those providing 3D-structural (LIDAR, SAR) and hyperspectral information becoming increasingly available with longer and more temporally dense time series, studying ecosystems dynamics (that is, spatial and temporal variation in ecological processes) can be substantially improved, which will lead to a better understanding of ecosystem resilience. Case study examples have shown the value of using temporal autocorrelation or mapping the rate and speed of

recovery after disturbances to quantify resilience directly from remotely sensed data (Verbesselt et al., 2016, Senf, 2022). The ever-increasing length of remote sensing time series on the matter of decades underpins a new comprehensive assessment of ecosystem dynamics including the identification of critical changes in ecosystem resilience directly through monitoring disturbance frequency and recovery rates over time and underpin rapid/near real time monitoring and development of early warning signals for critical transitions to occur (Senf 2022).

From an EO-data perspective, one of the most important goals is to provide time series that are as long and as temporally dense as possible. It is essential here to make use and ensure the long-term continuity and consistency of all observations from Landsat and Sentinels 1,2 to capture vegetation dynamics and using various sensors capturing vegetation structure dynamics and soil moisture dynamics globally (like SMOS). In addition, land surface temperature (i.e. Landsat, LSTM), albedo and water vapour are critical variables. Increasingly, we are also interested in the functional behaviour of vegetation systems and the land surface and land surface cover more generally, and the important role that this plays in the ecology, biodiversity and sustainability of the ecosystem based on it. This requires a much better knowledge of the physical behaviour of the vegetation canopy and its conditions, and the local environment. This means that not only vegetation types and distribution are required but parameters such as above ground biomass (AGB) and vegetation structure derived from LIDAR, passive/active microwave systems, solar induced fluorescence (SIF) from FLEX and biogeochemical characteristics from hyperspectral data (i.e. ENMAP, CHIME).

Comprehensive assessment of ecosystem dynamics, including a) the identification of critical changes in ecosystem resilience through monitoring disturbance frequency and b) assessing impacts and recovery rates over time requires improving the characterisation of critical parameters: i) vegetation canopy height, ii) vegetation fractional cover, iii) 3D canopy characterisation including canopy structure, layering, plant area at different heights and iv) canopy components (biomass distribution and geometry). These observations will lead to improving the understanding of links between vegetation characteristics and climate at relevant scales is crucial to informing ecosystem management, conservation efforts, and climate change mitigation strategies. Key variables are required to achieve this improvement, i) land surface temperature, ii) Earth surface albedo and iii) canopy water content.

4.3.2: Review the measurement specifications

Taking a new look into Earth Observations and the assessment of where and how ecosystems are undergoing critical transitions requires a series of integrated monitoring assets. This relates to both the comprehensive assessment of ecosystem dynamics including the identification of critical changes in ecosystem resilience directly through monitoring disturbance frequency, impacts and recovery rates over time and the understanding of links between vegetation characteristics and climate at relevant scales. The following observations are required, all with a global scope:

- Dense, long time series-based datasets from different optical, thermal and SAR sensors incl. Landsat, S1/2, SMOS etc. to track disturbance/regrowth dynamics as well as “stable” ecosystem characteristics. To go more towards the monitoring of “individuals” (i.e. trees), 5-10 m spatial

resolution for at least a 10-year history extent is needed. For longer-time series analysis and trends, the Landsat 30m archive should be used. Dense temporal resolution from weekly-monthly resolutions are preferred to track also short-term and small-scale events, including the importance of near-real time data delivery for alerting and early warning.

- For vegetation structural characteristics and changes (i.e. height, cover, 3-D structure, biomass) the following EO-based data sources are needed: very-high resolution optical data (< 1 m), regular space-based LIDAR and/or long-wave SAR (L-Band, P-Band). A combined approach capitalising on multiple sensing opportunities that capture vegetation structure and dynamics is preferred.
- Linking satellite and on-the ground monitoring: the remote sensing data analysis needs to be underpinned by site level local climate/vegetation experiments and regular campaigns (i.e. from ecosystem plots/networks), and/or near-sensing (drone, terrestrial) measurements, i.e. capitalising on LTER, ICOS, GEOTREES or STRUCNET sites. There is a need for additional, coordinated ground data acquisition campaigns on ecosystem disturbances and recovery (i.e. terrestrial/drones, citizen science). Statistical and AI methods should be explored for integrating EO data with the various sources of ground data.

4.3.3: Capabilities assessment of existing and planned missions

Improving EO-based methods and observations to assess critical transitions on ecosystems can focus on exploiting existing capabilities covering structure and composition and can capitalise on new EO missions. Only considering the synergy and interoperability of different novel EO-data streams allows for an increasingly comprehensive characterization of ecosystems and biodiversity. Quantify the structure as key feature of many terrestrial ecosystems and forest, for example, can take advantage of various space-based mission either operation or forthcoming (GEDI/ICESAT-2, Sentinel-1, BIOMASS, ROSE-L) that allow for much more detailed measurements of the three-dimensional structure at high resolution and at scales that also relate to ongoing on the ground ecological and forest monitoring networks. For characterising ecosystem composition, the recent arrival of space-based imaging spectroscopy (ENMAP, PRISMA, EMITS, CHIME) provides new opportunities. EO-based when combined with innovative ground data (i.e. eDNA, sound sensors, citizen science) can provide high resolution and accurate estimates of community composition. These approaches should be leveraged for a new global effort for characterising both ecosystem structures and composition and its relationships at local and regional level and its dynamics over time related to disturbance and regrowth trajectories. Most observation opportunities exist for forests and vegetated ecosystems; but under-studied ecosystems (IPBES, 2019) such as freshwater systems, Arctic, marine/ocean, seabed, and wetlands should also be considered.

From an observation perspective, using EO-systems operating now or in the coming years provide a lot of additional new information that still needs to be fully explored. Currently the interoperability of instruments in the optical domain such as the MultiSpectral Instrument (MSI) on-board Sentinel-2A & -2B and the Operational Land Imager 2 (OLI-2) on-board Landsat 9 has been demonstrated e.g. the Harmonized Landsat and Sentinel-2 (HLS) surface reflectance data set (Claverie et al., 2018; Crawford et al., 2023) and the ESA Sen2Like project has developed algorithms to generate harmonised 10m Landsat and Sentinel-2 products (Saunier et al., 2022). Consistent and systematic processing chains that make the

most of the available Landsat observations combined with Sentinel-2A, -2B and planned Sentinel-2C and -2D missions (Drusch et al., 2012) and Landsat Next (Masek et al, 2020) represents a unique opportunity to monitor land ecosystems. One key challenge is interoperability. Different instruments and observational datasets will be useful (optical, hyperspectral, SAR, LIDAR etc.) and make sure they can be analysed in conjunction and in a consistent manner is to be ensured. The same is true for integrating with space-based on on-the ground monitoring. There is a need for streamlining workflows from data collection to estimation and modelling across the different data streams and sources. High quality LIDAR/SAR observations are only available for recent years and will result in higher quality estimations. For long-term trends, the use of optical and SAR-based systems with a longer time series record is required. In the longer term, a more precise and repeatable (i.e., revisiting the same areas every year) space-borne LIDAR system could be developed to track ecosystem structure increasingly through time.

4.3.4: Discussion on the capability gaps

While ecosystems are undergoing rapid changes worldwide, a consistent, accurate and spatially detailed characterization of ecosystem structure and composition is largely lacking to date. Such information is essential to understand fundamental patterns of ecosystems and biodiversity and are needed to provide integrated information for guiding and assessing actions and policies aimed at managing and sustaining its many functions and benefits. In the recent assessment of EBV vs. remote sensing priorities (Skidmore et al., 2021), the variables focusing on the monitoring of ecosystem conditions (beyond just ecosystem extent) and structure (i.e. habitat structure, fragmentation etc.) have received a high score; considering that many of the top-ranking EBV's in that prioritisation study are also covered by Essential Climate Variables (ECVs). New Earth Observation sensors integrated with innovative ground sensing now provide the opportunities to address these issues towards a new era of monitoring ecosystems and critical transitions, including the understanding of long-term dynamics and towards near-real estimations and early warning. This allows us to go beyond identifying land cover or plant functional types but take advantage of a much wider variety of satellite and instrument combinations that can provide a wide range of information about land surface and ecosystem processes important for sustainability and managing ecological dynamics for a variety of key policies and climate smart land use practices.

A key piece of understanding currently missing is the need for better understanding of vegetation-climate interactions. At macro-climatic levels this has been addressed by the Earth System modelling community using coarse-scale data (i.e., MODIS and OLCI data). A key scientific question now is how microclimate is linked to micro-climate, that is the climate experienced by the local flora and fauna and also humans (Senf 2022). Micro-climate is often regulated by vegetation and spatially detailed remote sensing data of land surface temperature, albedo and water vapour can help linking vegetation characteristics to local climatic conditions, allowing to scale from the plot level (often monitored by ecologists) to more macro-Earth System models and global climate reanalysis data (e.g., Copernicus ERA5). Bridging information and process understanding across spatial and also temporal scales will improve monitoring the impacts of changing climates (and thus driving critical ecosystem changes) at levels important for species and individuals as well as humans. This knowledge generation and improved understanding of ecosystems critical transitions, from the observational point of view, can only be achieved by using a synergistic

approach where multiple EO-data streams with the adequate characteristics are used in an interoperable manner, see Figure 1.

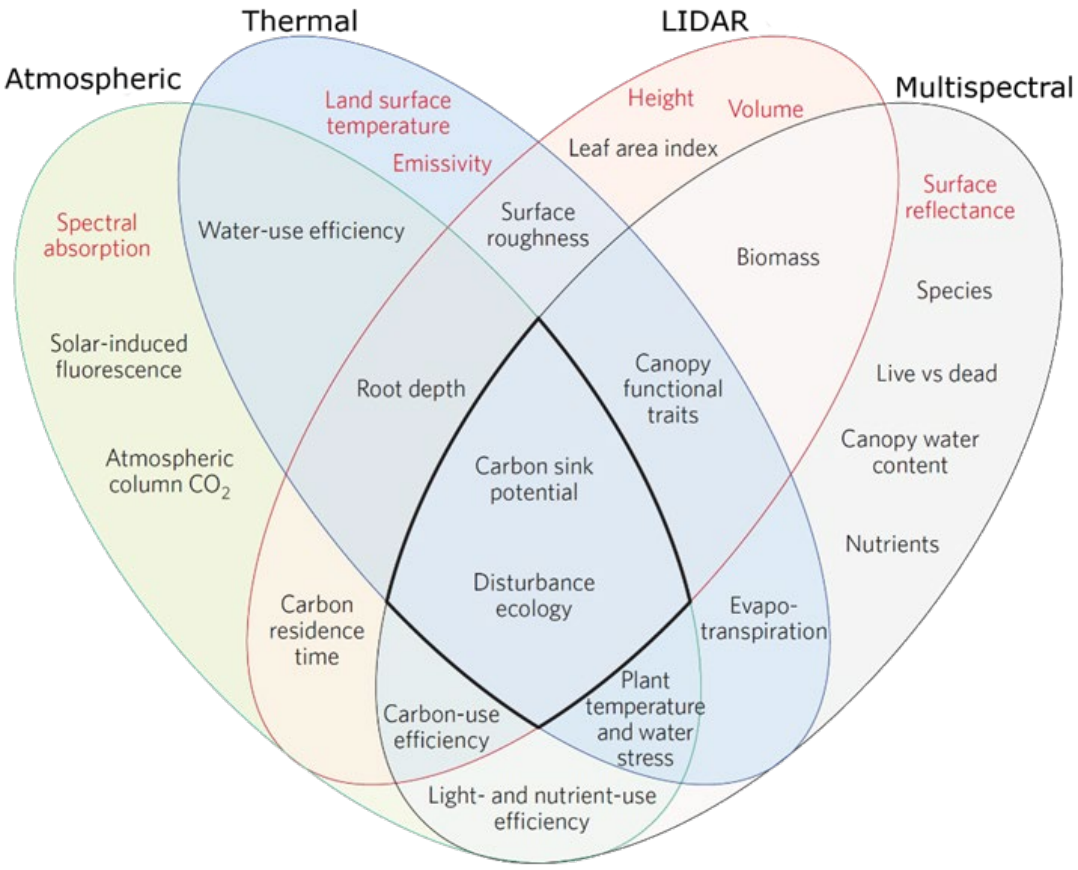

Figure 6: Synergy of different EO-based approaches for characterising Ecosystems and Biodiversity (adapted from Stavros et al., 2017).

5: Known Limitations

The contents of Deliverable 5 reflect the current state of study progress, which is dependent on a significant number of variables and inputs the study and science teams, and reflecting various states of progress across the scientific areas in the scope of the study.

The list of mapped Geophysical Observables reflects the current state of completeness of the CEOS Database, OSCAR/Variables, as well as the current state of technological development. There may yet be cases where these mappings can be further consolidated or combined to help refine the overall output.

Appendices

A: Example Candidate Science Question Science Sheet

Example shown is an excerpt from the science sheet for CSQ-001: What anthropogenic and natural processes are driving the global carbon cycle?

Question	Knowledge Advancement Objectives	Geophysical Observables [Links to database]	MIM Number	Measurement Specifications	Data sets, Methods, Tools & Models	Policies / Benefits
What anthropogenic and natural processes are driving the global carbon cycle?	**A) Quantify CO_2 and CH_4 emissions from both anthropogenic and natural sources and CO_2 removals from natural sinks on spatial scales from individual facilities or field plots to regional and global scales on seasonal time scales.**	**1. Critical Parameters** *Column-averaged atmospheric CO2 and CH4 dry air mole fractions (XCO2, XCH4) and their gradients.*			Atmospheric CO_2 and CH_4 retrieval algorithms Atmospheric flux inverse models	Integrated constraint on net emissions and removals of CO_2 and CH_4 for climate change (CC) mitigation and adaptation policy Climate finance. Monitor the efficacy of decarbonization policies and CO_2 removal strategies
		CO_2 Mole Fraction	CEOS 44	CO_2, CH_4 and O_2 bands at 1-10 km spatial resolution with 0.1 to 0.5% accuracy. CO_2, CH_4 observations with accuracies of 1-2% on spatial scales 0.01 to 1 km.		
		CO_2 Total Column	CEOS 274			
		CH_4 Mole Fraction	CEOS 39			
		CH_4 Total Column	CEOS 272			
		2. Supporting Parameters				
		Aerosols optical depth	CEOS 33	Aerosol and cloud measurements to mitigate biases. NO_2 and CO to identify plumes and discriminate wildfire from high-temperature combustion.		
		Cloud imagery	CEOS 109			
		Cloud cover	CEOS 111			
		NO_2 Mole Fraction	CEOS 74			
		CO Mole Fraction	CEOS 49			

Table A.1: Example Science Question Mapping Table

B: Geophysical Observables Unmapped to the CEOS Database or OSCAR Variables

This appendix contains a raw list of Geophysical Observables (GO) that were identified by the science teams, but are not mapped to either the CEOS Database, nor OSCAR. Noting that some of these GO may not be currently possible from space (as identified by the science teams), and others may require remapping to existing capabilities.

Geophysical Observable	**CSQ-KAO**
3-d canopy structure	CSQ-55, KAO-A; CSQ-56, KAO-A
Aerosols that contribute to effective radiative forcing	CSQ-46, KAO-B
Bedrock topography	CSQ-20, KAO-A; CSQ-20, KAO-B
Calving front location	CSQ-20, KAO-A; CSQ-20, KAO-B
Deep water formation	CSQ-24, KAO-A
Dissolved organic matter (dom)	CSQ-7, KAO-A; CSQ-7, KAO-B; CSQ-7, KAO-C
Earth surface temperature	CSQ-48, KAO-A; CSQ-48, KAO-C; CSQ-48, KAO-B
Euphotic depth	CSQ-25, KAO-B; CSQ-25, KAO-A
Fast ice extent	CSQ-21, KAO-A; CSQ-21, KAO-B
Ground displacements by GNSS	CSQ-38, KAO-A
Ground geophysical dataset: seismicity: support the development of arrays of seafloor seismometers.	CSQ-36, KAO-B; CSQ-36, KAO-C
Ground geophysical dataset: seismology, tsunami records from near-coastal pressure gauges and sea bottom pressure measurements: support the development of arrays of seafloor seismometers.	CSQ-36, KAO-D
Ground water	CSQ-44, KAO-C
Groundwater depletion	CSQ-44, KAO-B
Ice surface melt	CSQ-20, KAO-B; CSQ-20, KAO-A
Ice surface stress	CSQ-21, KAO-A; CSQ-21, KAO-B
Irrigated areas	CSQ-44, KAO-A
Land ice surface temperature	CSQ-48, KAO-B; CSQ-48, KAO-A; CSQ-48, KAO-C
Latent heat flux	CSQ-48, KAO-B; CSQ-48, KAO-C; CSQ-43, KAO-D; CSQ-48, KAO-A
Latent heat flux at earth surface	CSQ-45, KAO-A
Lead fraction	CSQ-21, KAO-B; CSQ-21, KAO-A

Geophysical Observable	CSQ-KAO
Leaf/canopy pigments	CSQ-55, KAO-B
Lithosphere thickness	CSQ-33, KAO-A; CSQ-33, KAO-B; CSQ-33, KAO-C
Melt ponds	CSQ-21, KAO-B; CSQ-21, KAO-A
Mixed layer depth	CSQ-25, KAO-A; CSQ-25, KAO-B
Net radiation	CSQ-48, KAO-A; CSQ-48, KAO-C; CSQ-48, KAO-B
Non-photosynthetic vegetation (npv) characterisation (hyperspectral)	CSQ-55, KAO-C
Ocean evaporation	CSQ-7, KAO-A; CSQ-7, KAO-C; CSQ-7, KAO-B
Ocean mass	CSQ-46, KAO-A
Permafrost depth	CSQ-24, KAO-A
Permafrost extent	CSQ-20, KAO-B; CSQ-20, KAO-A
Permafrost thawing	CSQ-20, KAO-A; CSQ-20, KAO-B
Planetary ocean and atmospheric heat transport	CSQ-48, KAO-C; CSQ-48, KAO-A; CSQ-48, KAO-B
Plant stress	CSQ-2, KAO-D
River discharge	CSQ-44, KAO-A
Sea bottom pressure measurements, GNSS-acoustic observation systems with high frequency of observation	CSQ-36, KAO-A
Seafloor displacements: sea bottom pressure measurements, GNSS-acoustic observation systems with high frequency of observation	CSQ-36, KAO-B; CSQ-36, KAO-D; CSQ-36, KAO-C; CSQ-36, KAO-E
Sensible heat flux	CSQ-43, KAO-D; CSQ-48, KAO-A; CSQ-48, KAO-B; CSQ-48, KAO-C
Sensible heat flux at earth surface	CSQ-45, KAO-A
Snow depth on ice	CSQ-21, KAO-B; CSQ-21, KAO-A
Snow melting rate	CSQ-20, KAO-B; CSQ-20, KAO-A
Stress under ice	CSQ-21, KAO-A; CSQ-21, KAO-B
Trace gases that contribute to effective radiative forcing (excluding co2)	CSQ-46, KAO-B
Vegetation canopy water content	CSQ-56, KAO-B
Vegetation water content	CSQ-43, KAO-A; CSQ-43, KAO-B; CSQ-2, KAO-A; CSQ-2, KAO-B; CSQ-2, KAO-D

Geophysical Observable	CSQ-KAO
Waves in sea-ice	CSQ-21, KAO-A; CSQ-21, KAO-B
2022 GCOS ECV variable Terrestrial Water Storage (TWS)	CSQ-44, KAO-A; CSQ-44, KAO-B; CSQ-44, KAO-C
GCOS ECV Groundwater	CSQ-44, KAO-A; CSQ-44, KAO-B; CSQ-44, KAO-C
GCOS ECV Terrestrial Water Storage (TWS)	CSQ-44, KAO-A; CSQ-44, KAO-B; CSQ-44, KAO-C
GCOS ECV Ice Sheet Mass Change	CSQ-44, KAO-A; CSQ-44, KAO-B; CSQ-44, KAO-C
GCOS ECV Glacier Mass Change	CSQ-44, KAO-A; CSQ-44, KAO-B; CSQ-44, KAO-C

Table B.1: Geophysical Observables unmapped to the CEOS Database measurements or OSCAR/Variables

C: Initial Capability Gap Estimates (see separate volume)

The full contents of Appendix C are a full set of initial capability gap analysis, and is provided as a separate document for all CEOS Database measurements which were linked to priority critical Geophysical Observables. An example initial capability gap analysis for 'wind profile (horizontal)' is shown below.

Wind profile (horizontal)

Date generated: 2023-11-24

Measurement Domain: Atmosphere

Measurement Category: Atmospheric Winds

Category description: *Measurements of atmospheric winds are of primary importance to weather forecasting, and as a variable in the study of global climate change. Upper air wind speed and direction is a basic element of the climate system that influences many other variables.*

Measurement definition: *Vertical profile of the horizontal vector component (2D) of the 3D wind vector - Requested from surface to TOA (layers: LT, HT, LS, HS&M) - Physical unit: [m/s] - Accuracy unit: [m/s] intended as vector error, i.e. the module of the vector difference between the observed vector and the true vector.*

CEOS Database entry for Wind profile (horizontal):
https://database.eohandbook.com/measurements/instruments.aspx?measurementTypeWMOID=5

OSCAR Variable page: https://space.oscar.wmo.int/variables/view/179

Related Candidate Science Question

ID	CSQ	KAO	Priority Level
48-A	How can we improve the monitoring and understanding of planetary heat exchange at regional scale, and which essential advancements can we achieve for research and monitoring on	Thermodynamic coupling of the Earth's surface and the atmosphere to analyze critical feedback mechanisms, particularly for small-scale processes and variations to allow for improved weather	Critical

	weather and climate patterns?	and climate predictability	
48-B	How can we improve the monitoring and understanding of planetary heat exchange at regional scale, and which essential advancements can we achieve for research and monitoring on weather and climate patterns?	Further develop better weather prediction on short time scales (2–12 weeks) aiming for advance warning of events such as heat waves and extreme precipitation, storms and long-term weather.	Critical
48-C	How can we improve the monitoring and understanding of planetary heat exchange at regional scale, and which essential advancements can we achieve for research and monitoring on weather and climate patterns?	Study the dynamic coupling for improved understanding of momentum and kinetic energy transfer between components of the Earth's system (ocean, atmosphere, cryosphere, land)	Critical

Heat Map Timeline

Year	Number of predicted operational instruments
2028 (5 years from now)	38
2031 (8 years from now)	37
2033 (10 years from now)	38

2038 (15 years from now)	38

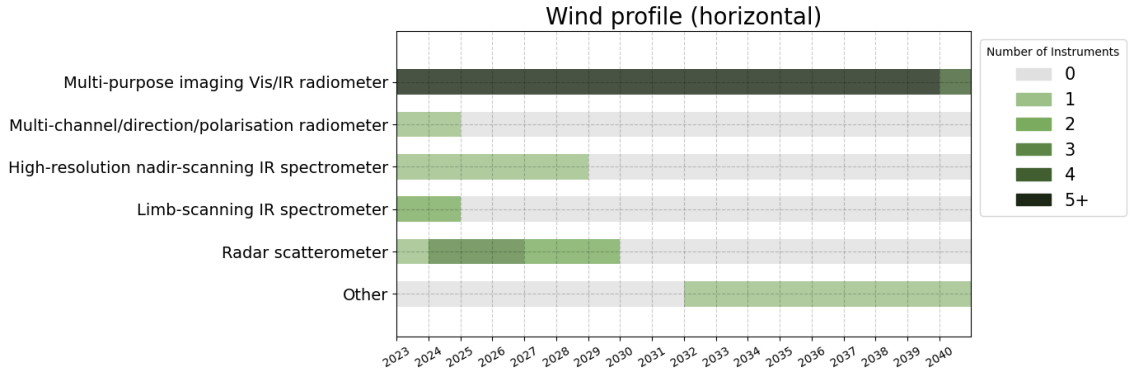

Detailed Timeline

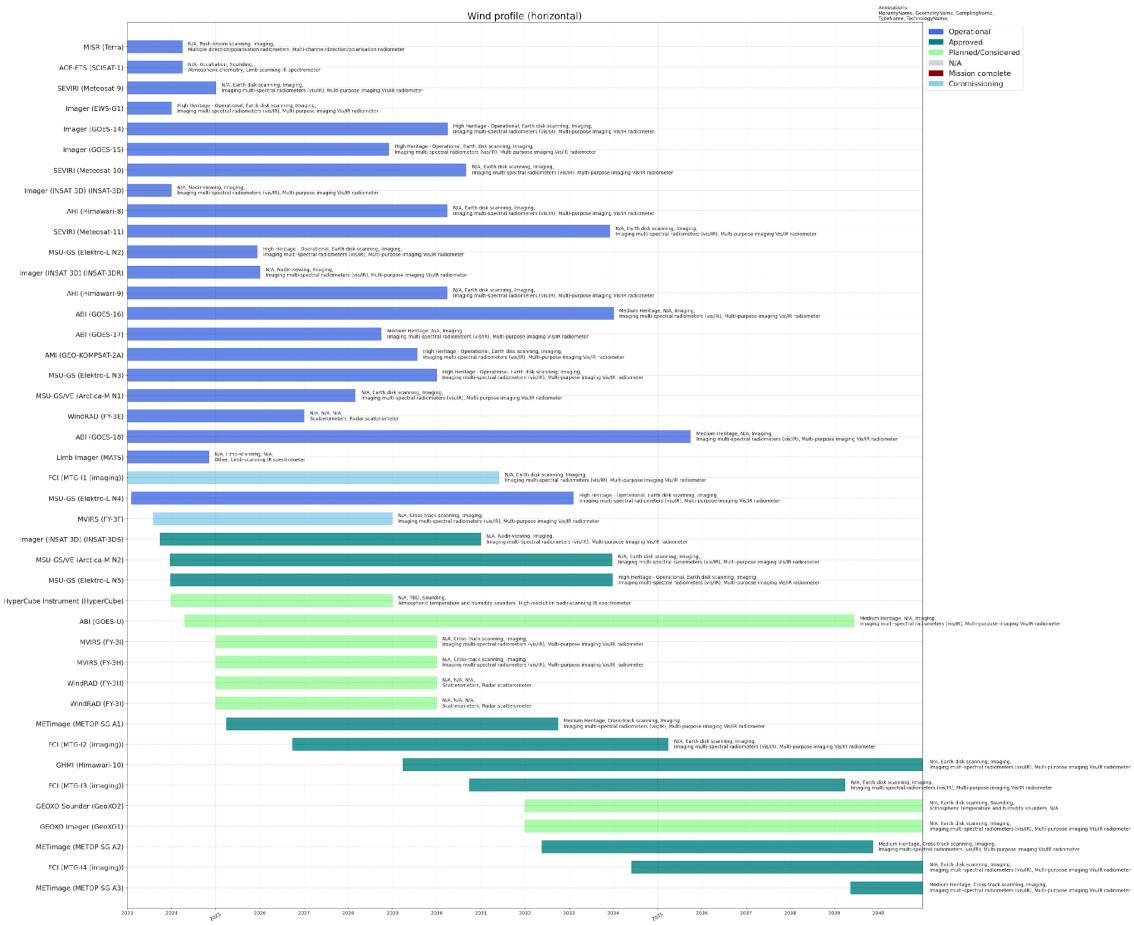

Instruments

Instruments recorded in ESSFS D4 as measuring Wind profile (horizontal)

Instrument	Utility (as assessed by agency)	Missions	CEOS DB Entry
SEVIRI	High Utility	Meteosat-9, Meteosat-10, Meteosat-11	https://database.eohandbook.com/database/instrumentsummary.aspx?instrumentID=302
Imager	High Utility	GOES-14, EWS-G1, GOES-15	https://database.eohandbook.com/database/instrumentsummary.aspx?instrumentID=331
MISR	High Utility	Terra	https://database.eohandbook.com/database/instrumentsummary.aspx?instrumentID=396
MSU-GS	High Utility	Elektro-L N2, Elektro-L N3, Elektro-L N4, Elektro-L N5	https://database.eohandbook.com/database/instrumentsummary.aspx?instrumentID=784
METimage	High Utility	METOP-SG A2, METOP-SG A3, METOP-SG A1	https://database.eohandbook.com/database/instrumentsummary.aspx?instrumentID=965
AMI	High Utility	GEO-KOMPSAT-2A	https://database.eohandbook.com/database/instrumentsummary.aspx?instrumentID=1575

WindRAD	High Utility	FY-3H, FY-3I, FY-3E	https://database.eohandbook.com/database/instrumentsummary.aspx?instrumentID=1625
AHI	High Utility	Himawari-8, Himawari-9	https://database.eohandbook.com/database/instrumentsummary.aspx?instrumentID=1651
MSU-GS/VE	High Utility	Arctica-M N2, Arctica-M N1	https://database.eohandbook.com/database/instrumentsummary.aspx?instrumentID=1691
GEOXO Imager	High Utility	GeoXO1	https://database.eohandbook.com/database/instrumentsummary.aspx?instrumentID=2045
GEOXO Sounder	High Utility	GeoXO2	https://database.eohandbook.com/database/instrumentsummary.aspx?instrumentID=2049
ABI	General Utility	GOES-17, GOES-18, GOES-U, GOES-16	https://database.eohandbook.com/database/instrumentsummary.aspx?instrumentID=870
FCI	General Utility	MTG-I4 (imaging), MTG-I1 (imaging), MTG-I2 (imaging), MTG-I3 (imaging)	https://database.eohandbook.com/database/instrumentsumma

			ry.aspx?instrumentID=885
HyperCube Instrument	General Utility	HyperCube	https://database.eohandbook.com/database/instrumentsummary.aspx?instrumentID=2036
Limb Imager	General Utility	MATS	https://database.eohandbook.com/database/instrumentsummary.aspx?instrumentID=2041
GHMI	General Utility	Himawari-10	https://database.eohandbook.com/database/instrumentsummary.aspx?instrumentID=2067
MVIRS	Marginal Utility	FY-3H, FY-3I, FY-3F	https://database.eohandbook.com/database/instrumentsummary.aspx?instrumentID=671
ACE-FTS	Marginal Utility	SCISAT-1	https://database.eohandbook.com/database/instrumentsummary.aspx?instrumentID=701
Imager (INSAT 3D)	Marginal Utility	INSAT-3DR, INSAT-3D, INSAT-3DS	https://database.eohandbook.com/database/instrumentsummary.aspx?instrumentID=788

D: Full list of Geophysical Observable Marked as Critical Priority

Geophysical Observable ***CEOS DB, OSCAR Variables, or Unmapped***	**Number**
CEOS: Gravity field	16
CEOS: Gravity gradients	11
CEOS: Ice sheet topography	11
CEOS: Land surface imagery	9
CEOS: Ocean chlorophyll concentration	9
CEOS: Land surface topography	8
CEOS: Atmospheric specific humidity (column/profile)	8
CEOS: Atmospheric temperature (column/profile)	8
CEOS: Above Ground Biomass (AGB)	7
CEOS: Sea surface temperature	7
CEOS: Land surface temperature	6
CEOS: Ocean surface currents (vector)	6
CEOS: Ocean suspended sediment concentration	6
CEOS: Ocean temperature	6
CEOS: Chlorophyll Fluorescence from Vegetation on Land	6
CEOS: Vegetation Canopy (height)	6
CEOS: Sea Surface salinity	5
OSCAR: river discharge	5
Unmapped: Vegetation water content	5
CEOS: Coastal sea level (tide)	5
CEOS: Colour dissolved organic matter (CDOM)	5
CEOS: CO2 Mole Fraction	5
CEOS: Lake Surface Temperature	5
CEOS: Sea level	5
CEOS: Sea-ice cover	4
CEOS: Land cover	4

Geophysical Observable ***CEOS DB, OSCAR Variables, or Unmapped***	**Number**
CEOS: Ocean salinity	4
CEOS: CO2 Total Column	4
CEOS: Earth surface albedo	4
Unmapped: Seafloor displacements: Sea bottom pressure measurements, GNSS-acoustic observation systems with high frequency of observation	4
Unmapped: Sensible heat flux	4
CEOS: Wind stress	4
Unmapped: Latent heat flux	4
Unmapped: Dissolved organic matter (DOM)	3
Unmapped: Earth surface temperature	3
CEOS: Wind profile (horizontal)	3
CEOS: Wind profile (vertical)	3
OSCAR: River runoff	3
Unmapped: Land ice surface temperature	3
Unmapped: Planetary ocean and atmospheric heat transport	3
CEOS: Fire radiative power	3
CEOS: CH4 Mole Fraction	3
CEOS: Glacier topography	3
CEOS: Ocean velocity	3
CEOS: Air temperature (near surface)	3
CEOS: Sea surface heat flux	3
CEOS: Sea-ice sheet topography	3
CEOS: Sea-ice surface temperature	3
CEOS: Snow surface temperature	3
Unmapped:GCOS ECV Groundwater	3
Unmapped: GCOS ECV Terrestrial Water Storage (TWS)	3
Unmapped: GCOS ECV Ice Sheet Mass Change	3

Geophysical Observable ***CEOS DB, OSCAR Variables, or Unmapped***	**Number**
Unmapped: GCOS ECV Glacier Mass Change	3
CEOS: Snow water equivalent	2
CEOS: Upward long-wave irradiance at TOA	2
CEOS: Upward short-wave irradiance at TOA	2
CEOS: Upwelling (Outgoing) long-wave radiation at Earth surface	2
CEOS: Upwelling (Outgoing) Short-wave Radiation at the Earth Surface	2
CEOS: Sea-ice thickness	2
CEOS: Sea-ice type	2
CEOS: Sea-ice motion	2
CEOS: Fire fractional cover	2
CEOS: Leaf Area Index (LAI)	2
CEOS: Precipitation intensity at the surface (liquid or solid)	2
CEOS: Normalized Differential Vegetation Index (NDVI)	2
CEOS: Ocean subsurface dissolved oxygen concentration	2
CEOS: Cloud drop effective radius	2
CEOS: Fraction of Absorbed PAR (FAPAR)	2
CEOS: Geoid	2
CEOS: Glacier motion	2
CEOS: Dissolved inorganic carbon (DIC)	2
CEOS: Downward long-wave irradiance at Earth surface	2
CEOS: Downward short-wave irradiance at Earth surface	2
CEOS: Downwelling (Incoming) solar radiation at TOA	2
Unmapped: Permafrost extent	2
Unmapped: Snow depth on ice	2
Unmapped: Stress under ice	2
Unmapped: Waves in sea-ice	2
OSCAR: Sea-ice surface characteristics	2

Geophysical Observable ***CEOS DB, OSCAR Variables, or Unmapped***	**Number**
OSCAR: snow depth	2
Unmapped: 3-D canopy structure	2
OSCAR: permafrost	2
OSCAR: pH	2
Unmapped: bedrock topography	2
Unmapped: calving front location	2
CEOS: Snow cover	2
CEOS: Water vapour imagery	2
Unmapped: euphotic depth	2
Unmapped: Ground geophysical dataset: seismicity: Support the development of arrays of seafloor seismometers.	2
Unmapped: ice surface melt	2
Unmapped: ice surface stress	2
Unmapped: lead fraction	2
Unmapped: melt ponds	2
Unmapped: mixed layer depth	2
Unmapped: Non-Photosynthetic vegetation (NPV) characterisation (hyperspectral)	1
Unmapped: leaf/canopy pigments	1
Unmapped: Irrigated areas	1
Unmapped: Latent heat flux at Earth surface	1
Unmapped: Ground geophysical dataset: seismology, tsunami records from near-coastal pressure gauges and sea bottom pressure measurements: Support the development of arrays of seafloor seismometers.	1
Unmapped: Ground water	1
Unmapped: Hyperspectral surface reflectance	1
Unmapped: Ground displacements by GNSS	1
CEOS: Wind speed over sea surface (horizontal)	1
CEOS: Wind vector over sea surface (horizontal)	1

Geophysical Observable ***CEOS DB, OSCAR Variables, or Unmapped***	**Number**
Unmapped: deep water formation	1
Unmapped: Aerosols that contribute to effective radiative forcing	1
Unmapped: vegetation canopy water content	1
Unmapped: Sensible heat flux at Earth surface	1
Unmapped: Plant stress	1
Unmapped: Sea bottom pressure measurements, GNSS-acoustic observation systems with high frequency of observation	1
CEOS: Evapotranspiration	1
CEOS: Lake Area	1
CEOS: Lake level	1
CEOS: Cloud ice (column/profile)	1
CEOS: Cloud liquid water (column/profile)	1
CEOS: Cloud optical depth	1
CEOS: Cloud top height	1
CEOS: Cloud top temperature	1
CEOS: Cloud type	1
CEOS: CO Mole Fraction	1
CEOS: CH4 Total Column	1
CEOS: Cloud cover	1
CEOS: Aerosol effective radius (column/profile)	1
CEOS: Aerosol Extinction / Backscatter (column/profile)	1
CEOS: Precipitation Profile (liquid or solid)	1
CEOS: NO2 Mole Fraction	1
CEOS: Short-wave Earth surface bi-directional reflectance	1
CEOS: Vegetation Canopy (cover)	1
CEOS: Soil moisture in the roots region	1
CEOS: Surface Water Extent	1
Total	411

Table D.1: Geophysical Observables marked as priority 'critical'

E: Section 4 References

Brienen, R. J. W., Phillips, O. L., Feldpausch, T. R., Gloor, E., Baker, T. R., Lloyd, J., Lopez-Gonzalez, G., Monteagudo-Mendoza, A., Malhi, Y., Lewis, S. L., Vásquez Martinez, R., Alexiades, M., Álvarez Dávila, E., Alvarez-Loayza, P., Andrade, A., Aragão, L. E. O. C., Araujo-Murakami, A., Arets, E. J. M. M., Arroyo, L., Aymard C., G. A., Bánki, O. S., Baraloto, C., Barroso, J., Bonal, D., Boot, R. G. A., Camargo, J. L. C., Castilho, C. V., Chama, V., Chao, K. J., Chave, J., Comiskey, J. A., Cornejo Valverde, F., da Costa, L., de Oliveira, E. A., Di Fiore, A., Erwin, T. L., Fauset, S., Forsthofer, M., Galbraith, D. R., Grahame, E. S., Groot, N., Hérault, B., Higuchi, N., Honorio Coronado, E. N., Keeling, H., Killeen, T. J., Laurance, W. F., Laurance, S., Licona, J., Magnussen, W. E., Marimon, B. S., Marimon-Junior, B. H., Mendoza, C., Neill, D. A., Nogueira, E. M., Núñez, P., Pallqui Camacho, N. C., Parada, A., Pardo-Molina, G., Peacock, J., Peña-Claros, M., Pickavance, G. C., Pitman, N. C. A., Poorter, L., Prieto, A., Quesada, C. A., Ramírez, F., Ramírez-Angulo, H., Restrepo, Z., Roopsind, A., Rudas, A., Salomão, R. P., Schwarz, M., Silva, N., Silva-Espejo, J. E., Silveira, M., Stropp, J., Talbot, J., ter Steege, H., Teran-Aguilar, J., Terborgh, J., Thomas-Caesar, R., Toledo, M., Torello-Raventos, M., Umetsu, R. K., van der Heijden, G. M. F., van der Hout, P., Guimarães Vieira, I. C., Vieira, S. A., Vilanova, E., Vos, V. A., and Zagt, R. J., (2015). Long-term decline of the Amazon carbon sink, Nature, 519, 344–348, https://doi.org/10.1038/nature14283

Byrne, B., Baker, D. F., Basu, S., et al., National CO2 budgets (2015–2020) inferred from atmospheric CO2 observations in support of the global stocktake. Earth Syst. Sci. Data, 15, 963–1004, 2023. doi: 10.5194/essd-15-963-2023

Claverie, M., Ju, J., Masek, J.G., Dungan, J.L., Vermote, E.F., Roger, J.C., Skakun, S.V. and Justice, C., 2018. The Harmonized Landsat and Sentinel-2 surface reflectance data set. Remote sensing of environment, 219, pp.145-161. https://doi.org/10.1016/j.rse.2018.09.002

CO2M MRD: Copernicus CO 2 Monitoring Mission Requirements Document, EOP-SM/3088/YM-ym, 2020. https://esamultimedia.esa.int/docs/EarthObservation/CO2M_MRD_v3.0_20201001_Issued.pdf

Cook, A. J. & Vaughan, D. G. Overview of areal changes of the ice shelves on the Antarctic Peninsula over the past 50 years. The Cryosphere 4, 77–98 (2010).

Cornford, S. L. et al. Century-scale simulations of the response of the West Antarctic Ice Sheet to a warming climate. The Cryosphere 9, 1579–1600 (2015).

Cox, P. M., Pearson, D., Booth, B. B., Friedlingstein, P., Huntingford, C., Jones, C. D., and Luke, C. M., (2013). Sensitivity of tropical carbon to climate change constrained by carbon dioxide variability, Nature, 494, 341–344, https://doi.org/10.1038/nature11882

Crawford, C.J., Roy, D.P., Arab, S., Barnes, C., Vermote, E., Hulley, G., Gerace, A., Choate, M., Engebretson, C., Micijevic, E. and Schmidt, G., 2023. The 50-year Landsat collection 2 archive. Science of Remote Sensing, 8, p.100103. https://doi.org/10.1016/j.srs.2023.100103

Crisp, D.; Pollock, H.R.; Rosenberg, et al., The on-orbit performance of the Orbiting Carbon Observatory-2 (OCO-2) instrument and its radiometrically calibrated products. Atmos. Meas. Tech. 2017, 10, 59–81. doi: 10.5194/amt-10-59-2017

Davison, B. J., A. E. Hogg, T. Slater, R. Rigby, (2023), Annual mass budget of Antarctic ice shelves from 1997 to 2021, Science Advances, 9, 41, DOI: 10.1126/sciadv.adi0186.

Davison, B. J., Hogg, A. E., Rigby, R., Veldhuijsen, S., van Wessem, J. M., van den Broeke, M. R., Holland, P. R., Selley, H. L., and Dutrieux, P.: (2023b) Sea level rise from West Antarctic mass loss significantly modified by large snowfall anomalies, Nat. Commun., 14, https://doi.org/10.1038/s41467-023-36990-3, 2023b.

DeVries, T. The Ocean Carbon Cycle, Annual Reviews of Environment and Resources, 47, 317-341, 2022. doi: 10.1146/annurev-environ-120920-111307

Drusch, M., Del Bello, U., Carlier, S., Colin, O., Fernandez, V., Gascon, F., Hoersch, B., Isola, C., Laberinti, P., Martimort, P. and Meygret, A., 2012. Sentinel-2: ESA's optical high-resolution mission for GMES operational services. Remote sensing of Environment, 120, pp.25-36. https://doi.org/10.1016/j.rse.2011.11.026

Dutrieux, P. et al. Strong Sensitivity of Pine Island Ice-Shelf Melting to Climatic Variability. Science 343, 174–178 (2014).

Friedlingstein, P., O'Sullivan, M., Jones, M. W., Andrew, R. M., Bakker, D. C. E., Hauck, J., Landschützer, P., Le Quéré, C., Luijkx, I. T., Peters, G. P., Peters, W., Pongratz, J., Schwingshackl, C., Sitch, S., Canadell, J. G., Ciais, P., Jackson, R. B., Alin, S. R., Anthoni, P., Barbero, L., Bates, N. R., Becker, M., Bellouin, N., Decharme, B., Bopp, L., Brasika, I. B. M., Cadule, P., Chamberlain, M. A., Chandra, N., Chau, T.-T.-T., Chevallier, F., Chini, L. P., Cronin, M., Dou, X., Enyo, K., Evans, W., Falk, S., Feely, R. A., Feng, L., Ford, D. J., Gasser, T., Ghattas, J., Gkritzalis, T., Grassi, G., Gregor, L., Gruber, N., Gürses, Ö., Harris, I., Hefner, M., Heinke, J., Houghton, R. A., Hurtt, G. C., Iida, Y., Ilyina, T., Jacobson, A. R., Jain, A., Jarníková, T., Jersild, A., Jiang, F., Jin, Z., Joos, F., Kato, E., Keeling, R. F., Kennedy, D., Klein Goldewijk, K., Knauer, J., Korsbakken, J. I., Körtzinger, A., Lan, X., Lefèvre, N., Li, H., Liu, J., Liu, Z., Ma, L., Marland, G., Mayot, N., McGuire, P. C., McKinley, G. A., Meyer, G., Morgan, E. J., Munro, D. R., Nakaoka, S.-I., Niwa, Y., O'Brien, K. M., Olsen, A., Omar, A. M., Ono, T., Paulsen, M., Pierrot, D., Pocock, K., Poulter, B., Powis, C. M., Rehder, G., Resplandy, L., Robertson, E., Rödenbeck, C., Rosan, T. M., Schwinger, J., Séférian, R., Smallman, T. L., Smith, S. M., Sospedra-Alfonso, R., Sun, Q., Sutton, A. J., Sweeney, C., Takao, S., Tans, P. P., Tian, H., Tilbrook, B., Tsujino, H., Tubiello, F., van der Werf, G. R., van Ooijen, E., Wanninkhof, R., Watanabe, M., Wimart-Rousseau, C., Yang, D., Yang, X., Yuan, W., Yue, X., Zaehle, S., Zeng, J., and Zheng, B., (2023). Global Carbon Budget 2023, Earth Syst. Sci. Data, 15, 5301–5369, https://doi.org/10.5194/essd-15-5301-2023

Friedlingstein, P., O'Sullivan, M., Jones, M. W., et al..: Global Carbon Budget 2023, Earth Syst. Sci. Data, 15, 5301–5369, https://doi.org/10.5194/essd-15-5301-2023, 2023.

Gourmelen, N. et al. CryoSat-2 swath interferometric altimetry for mapping ice elevation and elevation change. Adv. Sp. Res. 62, 1226–1242 (2018).

Gsell, A.S., Scharfenberger, U., Özkundakci, D., Walters, A., Hansson, L.A., Janssen, A.B., Nõges, P., Reid, P.C., Schindler, D.E., Van Donk, E. and Dakos, V., (2016). Evaluating early-warning indicators of critical transitions in natural aquatic ecosystems. Proceedings of the National Academy of Sciences, 113(50), pp.E8089-E8095. https://doi.org/10.1073/pnas.1608242113

Hauck, J., Zeising, M., Le Quéré, C., Gruber, N., et al., Consistency and challenges in the ocean carbon sink estimate for the global carbon budget. Front. Mar. Sci. 7, 571720. doi: 10.3389/fmars.2020.571720

Hogg, A. E. & Gudmundsson, G. H. Impacts of the Larsen-C Ice Shelf calving event. Nat. Clim. Change 7, 540–542 (2017).

Hubau, W., Lewis, S. L., Phillips, O. L., Affum-Baffoe, K., Beeckman, H., Cuní-Sanchez, A., Daniels, A. K., Ewango, C. E. N., Fauset, S., Mukinzi, J. M., Sheil, D., Sonké, B., Sullivan, M. J. P., Sunderland, T. C. H., Taedoumg, H., Thomas, S. C., White, L. J. T., Abernethy, K. A., Adu-Bredu, S., Amani, C. A., Baker, T. R., Banin, L. F., Baya, F., Begne, S. K., Bennett, A. C., Benedet, F., Bitariho, R., Bocko, Y. E., Boeckx, P., Boundja, P., Brienen, R. J. W., Brncic, T., Chezeaux, E., Chuyong, G. B., Clark, C. J., Collins, M., Comiskey, J. A., Coomes, D. A., Dargie, G. C., de Haulleville, T., Kamdem, M. N. D., Doucet, J.-L., Esquivel-Muelbert, A., Feldpausch, T. R., Fofanah, A., Foli, E. G., Gilpin, M., Gloor, E., Gonmadje, C., Gourlet-Fleury, S., Hall, J. S., Hamilton, A. C., Harris, D. J., Hart, T. B., Hockemba, M. B. N., Hladik, A., Ifo, S. A., Jeffery, K. J., Jucker, T., Yakusu, E. K., Kearsley, E., Kenfack, D., Koch, A., Leal, M. E., Levesley, A., Lindsell, J. A., Lisingo, J., Lopez-Gonzalez, G., Lovett, J. C., Makana, J.-R., Malhi, Y., Marshall, A. R., Martin, J., Martin, E. H., Mbayu, F. M., Medjibe, V. P., Mihindou, V., Mitchard, E. T. A., Moore, S., Munishi, P. K. T., Bengone, N. N., Ojo, L., Ondo, F. E., Peh, K. S.-H., Pickavance, G. C., Poulsen, A. D., Poulsen, J. R., Qie, L., Reitsma, J., Rovero, F., Swaine, M. D., Talbot, J., Taplin, J., Taylor, D. M., Thomas, D. W., Toirambe, B., Mukendi, J. T., Tuagben, D., Umunay, P. M., van der Heijden, G. M. F., Verbeeck, H., Vleminckx, J., Willcock, S., Wöll, H., Woods, J. T., and Zemagho, L., (2020). Asynchronous carbon sink saturation in African and Amazonian tropical forests, Nature, 579, 80–87, https://doi.org/10.1038/s41586-020-2035-0

Humphrey, V., Berg, A., Ciais, P., Gentine, P., Jung, M., Reichstein, M., Seneviratne, S. I., and Frankenberg, C., (2021). Soil moisture–atmosphere feedback dominates land carbon uptake variability, Nature, 592, 65–69, https://doi.org/10.1038/s41586-021-03325-5

IPBES (2019): Global assessment report on biodiversity and ecosystem services of the Intergovernmental Science-Policy Platform on Biodiversity and Ecosystem Services. E. S. Senf C. (2022). Seeing the System from Above: The Use and Potential of Remote Sensing for Studying Ecosystem Dynamics, Ecosystems 25: 1719–1737, https://doi.org/10.1007/s10021-022-00777-2

Jenkins, A. et al. West Antarctic Ice Sheet retreat in the Amundsen Sea driven by decadal oceanic variability. Nat. Geosci. 11, 733–738 (2018).

Joughin, I. et al. Seasonal Speedup Along the Western Flank of the Greenland Ice Sheet. Science 320, 781–783 (2008).

Joughin, I. et al. Seasonal Speedup Along the Western Flank of the Greenland Ice Sheet. Science 320, 781–783 (2008).

Jung, M., Reichstein, M., Schwalm, C. R., Huntingford, C., Sitch, S., Ahlström, A., Arneth, A., Camps-Valls, G., Ciais, P., Friedlingstein, P., Gans, F., Ichii, K., Jain, A. K., Kato, E., Papale, D., Poulter, B., Raduly, B., Rödenbeck, C., Tramontana, G., Viovy, N., Wang, Y.-P., Weber, U., Zaehle, S., and Zeng, N., (2017). Compensatory water effects link yearly global land CO2 sink changes to temperature, Nature, 541, 516–520, https://doi.org/10.1038/nature20780

Karion, A., Sweeney, C., Tans, P. P. and Newberger, T. (2010). AirCore: An innovative atmospheric sampling system. Journal of Atmospheric and Oceanic Technology, 27, 1839–1853. doi:10.1175/2010JTECHA1448.1

Kataoka, F., Crisp, D., Taylor, et al., The Cross-Calibration of Spectral Radiances and Cross-Validation of CO2 Estimates from GOSAT and OCO-2. Remote Sensing, 9, 1158, 2017. doi: 10.3390/rs9111158

Keller, G. R., Rosenberg, R. A., Spiers, G.D., et al., Inflight Radiometric Calibration and Performance of the Orbiting Carbon Observatory 3 for Version 10 Products. IEEE Trans. Geosci. Remote Sens., 60, 2022. doi: 10.1109/TGRS.2022.3216825

Kuze, A., Taylor, T.E., Kataoka, F., et al., Long-term vicarious calibration of GOSAT short-wave sensors: Techniques for error reduction and new estimates of radiometric degradation factors. IEEE Trans. Geosci. Remote Sens. 2014, 52, 3991–4004. doi: 10.1109/TGRS.2013.2278696

Landschützer, P., Laruelle, G.G., Roobaert, A., Regnier, P., 2020. A uniform pCO2 climatology combining open and coastal oceans. Earth Syst. Sci. Data 12, 2537–2553. doi: 10.5194/essd-12-2537-2020

Lee, R. A. M., O'Dell, C. W., Wunch, D., et al., Preflight Spectral Calibration of the Orbiting Carbon Observatory 2, IEEE Trans. Geosci. Remote Sens., 55, 2499-2508, 2017. doi: 10.1109/TGRS.2016.2645614

Masek, J.G., Wulder, M.A., Markham, B., McCorkel, J., Crawford, C.J., Storey, J. and Jenstrom, D.T., 2020. Landsat 9: Empowering open science and applications through continuity. Remote Sensing of Environment, 248, p.111968. https://doi.org/10.1016/j.rse.2020.111968

McMillan M; Shepherd A; Sundal A; Briggs K; Muir A; Ridout A; Hogg AE; Wingham D (2014) Increased ice losses from Antarctica detected by CryoSat-2, Geophysical Research Letters, 41, pp.3899-3905. doi: 10.1002/2014GL060111.

Membrive, O., Crevoisier, C., Sweeney, C., et al., AirCore-HR: a high-resolution column sampling to enhance the vertical description of CH4 and CO2. Atmos. Meas. Tech., 10, 2163–2181, 2017. doi: 10.5194/amt-10-2163-2017

Mouginot, J., Rignot, E. & Scheuchl, B. Sustained increase in ice discharge from the Amundsen Sea Embayment, West Antarctica, from 1973 to 2013. Geophys. Res. Lett. 41, 1576–1584 (2014).

Nilsson, J., P. Vallelonga, S. B. Simonsen, L. Sandberg Sørensen, R. Forsberg, D. Dahl-Jensen, M. Hirabayashi, K. Goto-Azuma, C. S. Hvidberg, H. A. Kjær, K. Satow (2015) Greenland 2012 melt event effects on CryoSat-2 radar altimetry, Geophysical Review Letters, 42, 3919–3926, doi:10.1002/2015GL063296.

O'Dell, C. W., Eldering, A., Wennberg, P. O., et al., Improved retrievals of carbon dioxide from Orbiting Carbon Observatory-2 with the version 8 ACOS algorithm, Atmospheric Measurement Techniques, 11: 6539–6576, 2018. doi:10.5194/amt-11-6539-2018

Paul, F. et al. The glaciers climate change initiative: Methods for creating glacier area, elevation change and velocity products. (2015) doi:10.1016/J.RSE.2013.07.043.

R.J.W. Brewin, S. Sathyendranath, G. Kulk, et al. Ocean carbon from space: current status and priorities for the next decade. Earth Sci. Rev., 104386, 2023, doi: 10.1016/j.earscirev.2023.104386.

Rignot, E. et al. Accelerated ice discharge from the Antarctic Peninsula following the collapse of Larsen B ice shelf. Geophys. Res. Lett. 31, 2–5 (2004).

Rignot, E., Mouginot, J. & Scheuchl, B. Ice Flow of the Antarctic Ice Sheet. Science 333, 1427–1430 (2011).

Rott, H., Skvarca, P. & Nagler, T. Rapid Collapse of Northern Larsen Ice Shelf, Antarctica. Science 271, 788–792 (1996).

Saunier, S., Pflug, B., Lobos, I.M., Franch, B., Louis, J., De Los Reyes, R., Debaecker, V., Cadau, E.G., Boccia, V., Gascon, F. and Kocaman, S., 2022. Sen2Like: Paving the way towards harmonization and fusion of optical data. Remote Sensing, 14(16), p.3855. https://doi.org/10.3390/rs14163855

Schlund, M., Wenzel, A., Camarretta, N., Stiegler, C. and Erasmi, S., (2023). Vegetation canopy height estimation in dynamic tropical landscapes with TanDEM-X supported by GEDI data. Methods in Ecology and Evolution, 14(7), pp.1639-1656. https://doi.org/10.1111/2041-210X.13933

Shepherd, A. et al. Mass balance of the Antarctic Ice Sheet from 1992 to 2017. Nature 558, 219–222 (2018).

Shepherd, A. et al. Trends in Antarctic Ice Sheet Elevation and Mass. Geophys. Res. Lett. 46, 8174–8183 (2019).

Siegert. M. J., M. J. Bentley, A. Atkinson, T. J. Bracegirdle, P. Convey, B. Davies, R. Downie, A. E. Hogg, C. Holmes, K. A. Hughes, M. P. Meredith, N. Ross, J. Rumble, Jeremy Wilkinson, (2023) Antarctic extreme events, Frontiers in Environmental Science, 11, 1229283, doi.org/10.3389/fenvs.2023.1229283.

Skidmore, A. et al., (2021). Priority list of biodiversity metrics to observe from space, Nature Eco Evo, 5, 896–906, https://doi.org/10.1038/s41559-021-01451-x

Skidmore, A.K., Coops, N.C., Neinavaz, E. et al. Priority list of biodiversity metrics to observe from space. Nat Ecol Evol 5, 896–906 (2021). https://doi.org/10.1038/s41559-021-01451-x

Slater, T., Hogg, A. E. & Mottram, R. Ice-sheet losses track high-end sea-level rise projections. Nat. Clim. Change 10, 879–881 (2020).

Slater, T., Lawrence, I. R., Otosaka, I. N., Shepherd, A., Gourmelen, N., Jakob, L., Tepes, P., Gilbert, L., and Nienow, P.: Review article: Earth's ice imbalance, Cryosphere, 15, 233–246, https://doi.org/10.5194/tc-15-233-2021, 2021.

Staal, A., Tuinenburg, O.A., Bosmans, J.H., Holmgren, M., van Nes, E.H., Scheffer, M., Zemp, D.C. and Dekker, S.C., (2018). Forest-rainfall cascades buffer against drought across the Amazon. Nature Climate Change, 8(6), pp.539-543. https://doi.org/10.1038/s41558-018-0177-y

Stavros, E.N., Schimel, D., Pavlick, R., Serbin, S., Swann, A., Duncanson, L., Fisher, J.B., Fassnacht, F., Ustin, S., Dubayah, R. and Schweiger, A., 2017. ISS observations offer insights into plant function. Nature Ecology & Evolution, 1(7), p.0194. https://doi.org/10.1038/s41559-017-0194

Strozzi, T., Luckman, A., Murray, T. & Wegmuller, U. Glacier Motion Estimation Using SAR Offset-Tracking Procedures. Geosci. Remote Sens. IEEE Trans. On 40, 2384–2391 (2002).

Surawy-Stepney, T., Hogg, A. E., Cornford, S. L. & Davison, B. J. Episodic Dynamic Change Linked to Damage on the Thwaites Glacier Ice Tongue from 2015 to 2021. Nature Geoscience, (2023).

Taylor, T. E., O'Dell, C. W., Baker, D., et al., Evaluating the consistency between OCO-2 and OCO-3 XCO2 estimates derived from the NASA ACOS version 10 retrieval algorithm. Atmos. Meas. Tech., 16, 3173–3209, 2023. doi: 10.5194/amt-16-3173-2023

van Wessem, J. M. et al. Modelling the climate and surface mass balance of polar ice sheets using RACMO2 – Part 2: Antarctica (1979–2016). The Cryosphere 12, 1479–1498 (2018).

Verbesselt J. et al. (2016). Remotely sensed resilience of tropical forests. Nature Climate Change 6:1028–1031.

Wallis, B. J., A. E. Hogg, J. M. van Wessem, B. J. Davison, M. R. van den Broeke, (2023), Widespread seasonal speed-up of west Antarctic Peninsula glaciers from 2014 to 2021, Nature Geoscience, 16, 231-237, doi.org/10.1038/s41561-023-01131-4.

Woolf, D. K., P. E. Land, J. D. Shutler, L. M., et al., On the calculation of air-sea fluxes of CO2 in the presence of temperature and salinity gradients, J. Geophys. Res. Oceans, 121, 1229–1248, 2016. doi:10.1002/2015JC011427

Wunch, D., Toon, G. C., Blavier, et al., The total carbon column observing network, Philosophical Transactions of the Royal. Society A, 369, 2087–2112, 2011. doi:10.1098/rsta.2010.0240

Wunch, D., Wennberg, P. O., Osterman, et al., Comparisons of the Orbiting Carbon Observatory-2 (OCO-2) XCO2 measurements with TCCON, Atmospheric Measurement Techniques, 10, 2209–2238, 2017. doi: 10.5194/amt-10-2209-2017